

## Research Paper

# Cell-penetrating Peptide-modified Targeted Drug-loaded Phase-transformation Lipid Nanoparticles Combined with Low-intensity Focused Ultrasound for Precision Theranostics against Hepatocellular Carcinoma

Hongyun Zhao<sup>1,2\*</sup>, Meng Wu<sup>3\*</sup>, Leilei Zhu<sup>2</sup>, Yi Tian<sup>4</sup>, Mingxing Wu<sup>5</sup>, Yizhen Li<sup>2</sup>, Liming Deng<sup>2</sup>, Wei Jiang<sup>2,6</sup>, Wei Shen<sup>1</sup>, Zhigang Wang<sup>2</sup>, Zhechuan Mei<sup>1,2</sup>, Pan Li<sup>2,7</sup>, Haitao Ran<sup>2,7</sup>, Zhiyi Zhou<sup>2,8</sup>, Jianli Ren<sup>2,7</sup>

1. Department of Gastroenterology, The Second Affiliated Hospital of Chongqing Medical University, Chongqing400010, P.R. China.
2. Chongqing Key Laboratory of Ultrasound Molecular Imaging, The Second Affiliated Hospital of Chongqing Medical University, Chongqing400016, P.R. China.
3. Department of Ultrasound, Zhongnan Hospital of Wuhan University, Wuhan, Hubei 430071, China.
4. Department of Plastic Surgery, The Second Affiliated Hospital of Chongqing Medical University, Chongqing400010, P.R. China.
5. Department of Ophthalmology, The Second Affiliated Hospital of Chongqing Medical University, Chongqing400010, P.R. China.
6. Department of Radiology, The Second Affiliated Hospital of Chongqing Medical University, Chongqing 400010, China.
7. Department of Ultrasound, The Second Affiliated Hospital of Chongqing Medical University, Chongqing 400010, China.
8. Department of Geriatrics, Chongqing General Hospital, Chongqing 400014, China.

\* Co-first Authors

✉ Corresponding author: Dr. Jianli Ren, Chongqing Key Laboratory of Ultrasound Molecular Imaging, No. 1 Yixueyuan Road, Yuzhong District, Chongqing400016, P.R. China. Email: 302111@hospital.cqmu.edu.cn and Dr. Zhiyi Zhou, Department of Geriatrics, Chongqing General Hospital, Chongqing 400014, P.R. China. Email: zzy16966@163.com

© Ivyspring International Publisher. This is an open access article distributed under the terms of the Creative Commons Attribution (CC BY-NC) license (<https://creativecommons.org/licenses/by-nc/4.0/>). See <http://ivyspring.com/terms> for full terms and conditions.

Received: 2017.08.15; Accepted: 2018.01.09; Published: 2018.02.14

## Abstract

**Objective:** Prepare a multifunctional ultrasound molecular probe, hyaluronic acid-mediated cell-penetrating peptide-modified 10-hydroxycamptothecin-loaded phase-transformation lipid nanoparticles (HA/CPPs-10-HCPT-NPs), and to combine HA/CPPs-10-HCPT-NPs with low-intensity focused ultrasound (LIFU) for precision theranostics against hepatocellular carcinoma (HCC).

**Methods:** HA/CPPs-10-HCPT-NPs were prepared using thin-film dispersion, ultrasound emulsification, and electrostatic effects. HA/CPPs-10-HCPT-NPs were characterized for particle size, zeta potential, encapsulation efficiency and drug-loading efficiency. *In vitro*, HA/CPPs-10-HCPT-NPs were tested for acoustic droplet vaporization (ADV) at different time points/acoustic intensities; the ability of HA/CPPs-10-HCPT-NPs to target SMMC-7721 cells was detected by confocal laser scanning microscopy (CLSM); the penetrating ability of CG-TAT-GC-modified NPs was verified by CLSM in a 3D multicellular tumor spheroid (MCTS) model; the effect of HA/CPPs-10-HCPT-NPs combined with LIFU on killing SMMC-7721 cells was measured by CCK-8 and flow cytometry. *In vivo*, the tumor-target efficiency of HA/CPPs-10-HCPT-NPs was evaluated by a small-animal fluorescence imaging system and CLSM; the enhanced ultrasound imaging efficiency of HA/CPPs-10-HCPT-NPs combined with LIFU was measured by an ultrasound imaging analyzer; the therapeutic effect of HA/CPPs-10-HCPT-NPs combined with LIFU was evaluated by tumor volume, tumor inhibition rate, and staining (hematoxylin and eosin (H & E), proliferating cell nuclear antigen (PCNA) and TUNEL).

**Results:** Mean particle size and mean zeta potential of HA/CPPs-10-HCPT-NPs were  $284.2 \pm 13.3$  nm and  $-16.55 \pm 1.50$  mV, respectively. HA/CPPs-10-HCPT-NPs could bind to SMMC-7721 cells more readily than CPPs-10-HCPT-NPs. Penetration depth into 3D MCTS of HA/CPPs-10-HCPT-NPs was 2.76-fold larger than that of NPs without CG-TAT-GC. HA/CPPs-10-HCPT-NPs could enhance

ultrasound imaging by undergoing ADV triggered by LIFU. HA/CPPs-10-HCPT-NPs+LIFU group demonstrated significantly higher efficiency of anti-proliferation and apoptosis percentage than all other groups. In mouse liver tumor xenografts, HA/CPPs-10-HCPT-NPs could target tumor sites and enhance ultrasound imaging under LIFU. HA/CPPs-10-HCPT-NPs+LIFU group had a significantly smaller tumor volume, lower proliferative index (PI), and higher tumor inhibition and apoptotic index (AI) than all other groups.

**Conclusions:** Combined application of HA/CPPs-10-HCPT-NPs and LIFU should be a valuable and promising strategy for precise HCC theranostics.

Key words: Hepatocellular carcinoma; cell-penetrating peptide; phase-transformation; low-intensity focus ultrasound; ultrasound molecular imaging; theranostics

## Introduction

Worldwide, hepatocellular carcinoma (HCC) is the fifth most prevalent cancer type and the third most deadly [1–3]. Optimal treatment for HCC is radical resection, but many HCC patients have advanced HCC or distant metastasis, so treatment is challenging and the prognosis poor [4]. Due to the poor sensitivity of HCC to existing chemotherapy drugs, the effect is unsatisfactory [4, 5]. Thus, there is a critical, unmet need to explore new target sites and new methods to develop new drugs to diagnose and treat HCC.

The ultrasound contrast agents “ultrasound microbubbles” have been used widely for the diagnosis/differential diagnoses of diseases [6–8], especially liver diseases [9]. Ultrasound microbubbles are also used widely in experimental research as vehicles for carrying anti-cancer drugs or genes [10–12]. However, due to their micro-sized dimensions, ultrasound microbubbles cannot penetrate the vascular endothelial space of the tumor (380–780 nm) [13, 14] and the imaging and treatment of the extravascular tumor tissue is difficult [15]. Lipid nanoparticles (NPs) were developed to address this dilemma. As anti-cancer drug carriers, lipid NPs can penetrate the vascular endothelial gaps of tumors and deliver chemotherapy drugs to tumor tissue. However, conventional lipid NPs enhance backscattering depending on the gathering of NPs, and the imaging effect is inferior to that of ultrasound microbubbles [16]. In recent years, several studies have indicated that phase-transformation lipid NPs coated with liquid perfluoropentane (PFP) can elicit ADV. Using a certain intensity of external ultrasonic irradiation, PFP-coated lipid NPs can be changed into lipid microbubbles to enhance ultrasound imaging [14, 15, 17].

Cell-penetrating peptides (CPPs; also called the “protein transduction domains”) can deliver macromolecular substances (e.g., proteins, polypeptides, nucleic-acid fragments) directly and actively through cellular membranes into the cytoplasm or nucleus without causing cytotoxicity

[18, 19]. CPPs have high affinity for cell membranes and permeate the membranes quickly without destroying cell structures or degrading rapidly [20]. The human immunodeficiency virus type-1 transactivating transcriptional activator (HIV-1 TAT) protein is one of the most popular CPPs. As one of the shortest peptides, TAT can translocate across membranes into cell nuclei without causing cytotoxicity [18, 21]. TAT peptide (TATp)-modified nanocarriers (e.g., liposomes, micelles) can deliver various drugs and genes into cells *in vitro* and *in vivo* [20, 22]. Studies from our research team [20, 23, 24] have shown the novel cysteine-flanked cell-penetrating peptide CG-TAT-GC to have better penetration than the unmodified form of TAT, but is non-specific. Therefore, such non-specific CPPs need to have a targeted “guidance system” to reach the target site.

Common lipid NPs lack specific targets and the number of NPs reaching the target site actively are few, so effective molecular imaging and targeted therapy is challenging. Targeted NPs need to be developed to overcome this problem. The targeting strategies include ligands-mediated active targeting and ultrasound or radiofrequency-mediated passive targeting [25–27]. The human hepatoma SMMC-7721 cell membrane overexpresses cluster of differentiation (CD)44 [28]. This is a cell adhesion factor with a molecular weight of 82 kDa. CD44 is related to the genesis, invasion, and metastasis of tumor cells to the lymph nodes. Importantly, CD44 can bind hyaluronic acid (HA) specifically [29, 30] and is a potential target for the treatment of liver cancer. HA has non-immune characteristics, good biocompatibility and bio-degradability, and is a natural macromolecular polysaccharide [27, 31]. HA has high affinity for the specific overexpressed markers present on the surface of tumor cells such as CD44 [30]. In addition, when conjugated with drugs, HA can enhance the endocytosis mediated by receptors, making the drug target focal areas actively, avoiding toxicity to normal cells and improving its therapeutic index [27].

Hyaluronidase (HAase) is distributed widely in the acidic extracellular matrix of tumor cells and can hydrolyze HA to expose CPPs in HA-coated NPs [27, 32]. NPs modified by specific substances have been shown to be promising vectors for targeting cells and tissues and to be effective deliverers of chemotherapy drugs [4, 33, 34].

10-hydroxy camptothecin (10-HCPT) is a broad-spectrum anti-cancer agent. The required dose of 10-HCPT for antitumor therapy is >20-times lower than that of paclitaxel or doxorubicin [35, 36]. 10-HCPT is a cell cycle-specific drug that selectively inhibits DNA topoisomerase (TOPO I) [37]. 10-HCPT is used mainly to treat cancer of the liver, stomach, head, neck as well as leukemia. However, 10-HCPT has limited application in the clinic owing to its low aqueous solubility, instability, and because it leads to nausea, vomiting, bone-marrow suppression and other adverse effects [38]. Studies have shown that chemotherapy drugs encapsulated by liposomes can reduce their toxicity as well as improve their stability and efficacy [10, 39–41].

“Low-intensity focused ultrasound” (LIFU) is a system developed by our research team that integrates diagnosis, treatment, monitoring, and efficacy evaluation. Studies have shown that LIFU has a precise focusing effect, does not damage surrounding normal tissue, and leads to

quantitatively controlled release from drug-delivery systems [15, 42]. In addition, LIFU has good penetration and anti-attenuation, which conventional diagnostic ultrasound does not have. Ultrasound-targeted microbubble destruction (UTMD) is a passive targeting strategy used widely to promote gene transfection, drug delivery, and increased capillary permeability [43–46].

Here, we wished to develop a new precise system for the diagnosis and treatment of HCC based on a novel multifunctional ultrasound molecular probe combined with LIFU. As shown in the schematic diagram (Figure 1), hyaluronic acid-mediated cell-penetrating peptide-modified 10-hydroxycamptothecin-loaded phase-transformation lipid nanoparticles (HA/CPPs-10-HCPT-NPs) mediated by HA accumulated in tumor tissues near tumor vessels through the vascular endothelial gaps after injection (though the tail vein) of mice. HA on the surface layer of HA/CPPs-10-HCPT-NPs was degraded by HAase, and CPPs were exposed in a HAase-rich tumor microenvironment. CPPs-10-HCPT-NPs could penetrate deep into tumor tissue and cells through the stroma and cell membranes of tumor cells. After irradiation by LIFU, NPs in tumor tissue and cells turned into microbubbles after ADV, thereby enhancing ultrasound imaging at the cellular level. Soon afterwards, LIFU triggered microbubble

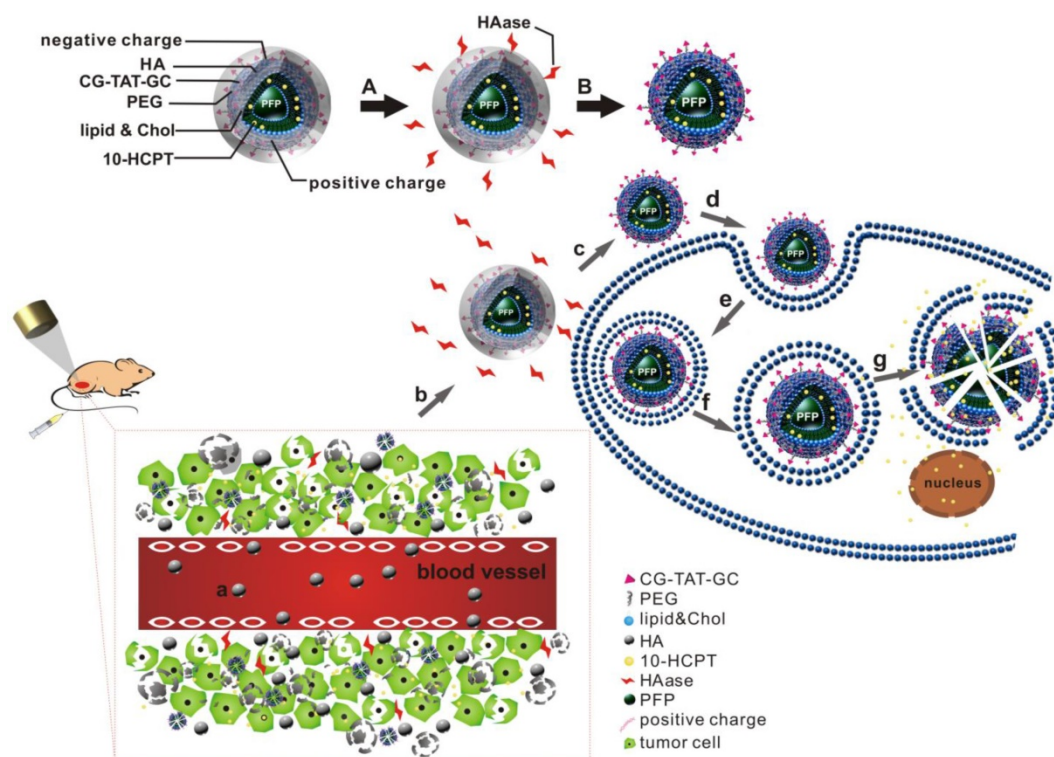


**Figure 1.** Combined application of HA/CPPs-10-HCPT-NPs and LIFU for precise theranostics of liver cancer (schematic). (A) Degradation of HA by HAase. (B) Disassembly of HA/CPPs-10-HCPT-NPs to CPPs-10-HCPT-NPs. (a) NPs injected intravenously in blood vessels. (b) NP accumulation at the tumor site via active and passive targeting. (c) Degradation of HA by HAase and exposure of CPPs in a HAase-rich tumor microenvironment. (d) CPPs induce uptake of NPs in SMMC-7721 cells. (e) Internalization of NPs into SMMC-7721 cells. (f) Generation of ADV by LIFU irradiation. (g) Explosion of NPs triggered by UTMD to promote drug release in the cytoplasm and nucleus.

rupture and promoted local release of antitumor drug, thereby realizing physicochemical synergistic treatment of the tumor. Our results showed, conclusively, that HA/CPPs-10-HCPT-NPs + LIFU could realize the early, precise and visual theranostics of liver cancer.

## Materials and Methods

### Materials and animals

1,2-Dipalmitoyl-sn-glycero-3-phosphatidylcholine (DPPC) and 3-(N-(N',N'-Dimethylaminoethane) carbamoyl) cholesterol (DC-Chol) were purchased from Avanti Polar Lipids (Alabaster, AL, USA). CG-TAT-GC (which had a sequence of CGYGRKKRRQRRRGC) was synthesized by ChinaPeptides (Beijing, China). DSPE-PEG-COOH was obtained from Nanocs (Boston, MA, USA). DSPE-PEG-CG-TAT-GC (DSPE-CPPs) was synthesized by Funuowei Biotechnology (Chongqing, China). 10-HCPT (purity =99.9%) was purchased from Lanbei Technology (Chengdu, China). An injection of 10-HCPT was obtained from Hubei Huangshi Feiyun Pharmaceuticals (Wuhan, China). Sodium hyaluronic acid (HA: molecular weight = 240 kDa) was purchased from Freda Biochem (Shandong, China). 1,1'-Diiodo-3,3',3',3'-tetramethylindocarbocyanine perchlorate (DiI) and 3,3'-diiodo-3,3',3',3'-tetramethylindocarbocyanine perchlorate (DiO) were provided from Beyotime Biotechnology (Shanghai, China). Hyaluronidase (HAase), 4', 6-diamidino-2-phenylindole (DAPI) and 1,1'-Diiodo-3,3',3',3'-tetramethylindocarbocyanine iodide (DiR) were obtained from Sigma-Aldrich (Saint Louis, MO, USA). Dulbecco's modified Eagle's medium (DMEM) and fetal bovine serum (FBS) were purchased from Gibco Co. (Carlsbad, CA, USA). Penicillin-streptomycin was obtained from Boster Biology Technology (Wuhan, China). Cell Counting Kit 8 (CCK-8) was provided by Dojindo Molecular Technology (Tokyo, Japan). Methyl alcohol and trichloromethane were purchased from Chongqing Chuandong chemicals (Chongqing, China). All other reagents were of analytical grade and used as received.

A rotary vacuum evaporator (RE-52A) was purchased from Yarong (Shanghai, China), along with a sonicator (VCX-130; Sonics & Materials, Danbury, CT, USA) and centrifuge (5804R; Eppendorf, Hamburg, Germany). An inverted fluorescence microscope (IX53) was obtained from Olympus (Tokyo, Japan), along with a confocal laser scanning microscope (A1R-Si; Nikon, Tokyo, Japan) and transmission electron microscope (TEM) (H-7500; Hitachi, Tokyo, Japan). A microplate reader (ELX800; Bio-tek Instruments, Winooski, VT, USA), dynamic

light scattering analyzer (Malvern Instruments, Malvern, UK) and a LIFU instrument (LMSC051 ACA; Institute of Ultrasound Imaging, Chongqing Medical Sciences, Chongqing, China) were also obtained.

A human HCC line (SMMC-7721) was provided by the Chongqing Key Laboratory of Ultrasound Molecular Imaging (Chongqing, China). Balb/c nude mice (4 weeks; 18-22g) were obtained from the Laboratory Animal Center of Chongqing Medical University (Chongqing, China) and maintained in accordance with guidelines set by the Animal Care Committee of Chongqing Medical University.

### Cell and multicellular tumor spheroid (MCTS) cultures

SMMC-7721 cells were maintained in DMEM containing FBS (10% v/v), penicillin (100 U/mL) and streptomycin (100 µg/mL) at 37°C in a humidified incubator in an atmosphere of 5% CO<sub>2</sub>. Cells were digested by 0.25% trypsin when they were in the exponential growth phase for subsequent experiments. The cell numbers for all the experiments were determined using a hemocytometer.

Three-dimensional (3D) MCTS was cultured as described previously [47]. Briefly, SMMC-7721 cells were digested and centrifuged, and cells were resuspended in fresh cell culture medium to obtain a single-cell suspension. The concentration of cells was adjusted to  $2.5 \times 10^4$ /mL. The lid of the culture dish was inverted, and a cell suspension (20 µL) added gently to the dish lid. Then, 6 mL of phosphate-buffered saline (PBS) was added to the dish, and the dish was covered by the lid. The dish was placed in a humidified incubator (37°C, 5% CO<sub>2</sub>) for cultivation of MCTS. The dish was observed every 3 days and the culture medium replaced if necessary.

### Establishment of animal and tumor xenograft models

All nude mice were pathogen-free and allowed access to food and water *ad libitum*. Animal experiments were carried out with the permission of the Animal Ethical Commission of Chongqing Medical University.

To create a hepatic tumor xenograft model, nude mice were inoculated with SMMC-7721 cells ( $1 \times 10^6$  cells/100 µL, s.c.) resuspended in DMEM with free FBS into the dorsal flank. Tumor-bearing nude mice were allowed to grow under standard conditions for 20 days after tumor inoculation and used for subsequent experiments. Tumor volume (V) was determined by measuring the length (L) and width (W) of the tumor using vernier calipers, and calculated as  $V = L \times W^2/2$  [10, 48]. The mean tumor

volume reached  $\sim 0.512 \text{ cm}^3$  at 20 days after tumor inoculation before experimental studies began.

### Preparation of NPs

NPs were prepared by thin-film dispersion and ultrasound emulsification according to a procedure reported previously [15, 27]. Briefly, 10 mg of DPPC, 4 mg of DSPE-CPPs, 3 mg of DC-cholesterol and 2 mg of 10-HCPT were dissolved in 5 mL of methyl alcohol and 10 mL of trichloromethane, which were removed with a rotary vacuum evaporator (1 h, 50°C). A thin film of lipids was formed at the bottom of the flask. This film was hydrated in 4 mL of distilled water. After precooling in an ice bath and addition of 60  $\mu\text{L}$  of PFP, the suspension was emulsified in an ice-water bath using a sonicator (Sonics & Materials) at 125 W for 6min (5s on and 5s off). To remove free lipids and excess reactants, the NPs were centrifuged at  $8228 \times g$  for 5 min at 4°C and then washed in distilled water. The centrifugation and washing process were repeated thrice. CPPs-10-HCPT-NPs were obtained and then stored at 4°C until further use.

HA/CPPs-10-HCPT-NPs were obtained by adding CPPs-10-HCPT-NPs to 0.6 mg/mL HA solution (1:1, v:v).

10-HCPT-NPs and HA/10-HCPT-NPs were obtained by the same procedures described above, except that DSPE was used instead of DSPE-CPPs.

To prepare fluorescent NPs, 5  $\mu\text{L}$  of DiI or DiR fluorescent dye was added to the lipid solution before film formation with tinfoil to prevent light exposure.

### Characterization of NPs

The mean particle size and zeta potential of NPs were measured by a dynamic light scattering analyzer (Malvern Instruments). The particle distribution of NPs was observed using an optical microscope (Olympus) and confocal laser scanning microscope (Nikon). Morphologic characterization of NPs was done using a transmission electron microscope (TEM) (H-7500; Hitachi).

### Encapsulation efficiency (EE) and drug-loading efficiency (LE) of NPs

We wished to determine the EE and LE of the different formulations of 10-HCPT-loaded NPs. A high-performance liquid chromatography (HPLC) system was used to assay the 10-HCPT concentration in various 10-HCPT formulations dissolved in chloroform and methanol [38]. The EE was defined as the percentage of 10-HCPT encapsulated in the NPs from the total amount of 10-HCPT used initially. The LE was the percentage of 10-HCPT encapsulated in the NPs *versus* the total amount of NPs ( $n = 3$ ) [10].

### *In vitro* ADV and ultrasound imaging of HA/CPPs-10-HCPT-NPs

We wished to investigate the ADV of HA/CPPs-10-HCPT-NPs triggered by LIFU (1.0 MHz, focal length of 1.5 cm, duty cycle of 50%, pulse-wave mode) irradiation *in vitro*. First, 500  $\mu\text{L}$  of a HA/CPPs-10-HCPT-NPs nanoemulsion (1 mg/mL) was added to agar gel phantom (3% agar w/v in distilled water). An ultrasound coupling agent was filled between the agar gel phantom and the LIFU probe to ensure that the focus of LIFU sonication was at the center of the nanoemulsion. We investigated the time-dependent (1-4 min) and acoustic intensity-dependent (2, 2.4 and 2.8  $\text{W}/\text{cm}^2$ ) ADV of HA/CPPs-10-HCPT-NPs *in vitro*, respectively. We also explored the optimal parameters of ADV triggered by LIFU. The ultrasound images before LIFU irradiation were the control. After each irradiation, ultrasound images of the nanoemulsion in the agar gel phantom were obtained. Then, the echo intensities of the regions of interest in B-mode and contrast-enhanced ultrasound (CEUS) were calculated by an ultrasound imaging analyzer (DFY-II; Institute of Ultrasound Imaging) [15, 20].

### Targeting and penetration efficiency of HA/CPPs-10-HCPT-NPs *in vitro*

To evaluate the targeting capability of HA/CPPs-10-HCPT-NPs *in vitro*, SMMC-7721 cells were seeded in culture dishes at a certain concentration and cultured at 37°C with 5%  $\text{CO}_2$  in a humidified incubator. After 24 h, cells were divided into three groups: HA/CPPs-10-HCPT-NPs, CPPs-10-HCPT-NPs, HA/CPPs-10-HCPT-NPs+HAase. HA/CPPs-10-HCPT-NPs were mixed with an equal volume of 2 mg/mL HAase solution for 1 h. The corresponding DiI-labeled NPs were administered at the same 10-HCPT dose of 4mg/kg for each group. After 30 min, cells were washed thrice with PBS, fixed with 4% paraformaldehyde for 10 min, and then incubated with DiO and DAPI for 5 min each. After fixing and dye administration, the cells were washed thrice with PBS. Finally, the dishes were stored away from light and sent for confocal laser scanning microscopy (CLSM).

3D-MCTS was used to mimic NPs *in vivo* and to confirm the penetration ability of HA/CPPs-10-HCPT-NP [49]. HA/CPPs-10-HCPT-NPs and HA/10-HCPT-NPs were co-cultured with 3D MCTS for 1 h, washed thrice with cold PBS, and sent for CLSM. Multiple-level scans for 3D MCTS were done at 2  $\mu\text{m}$  intervals to measure penetration.

### Anti-proliferation assay

The anti-proliferation efficiency of a combination of HA/CPPs-10-HCPT-NPs and LIFU was assessed

by the CCK-8 assay. The concentration of SMMC-7721 cells was adjusted to  $3 \times 10^4$ /mL. A cell suspension (100  $\mu$ L) was seeded into each well of 96-well plates and cultured in an incubator overnight. Cells were divided into 12 groups: control, free10-HCPT, HA/CPPs-10-HCPT-NPs, CPPs-10-HCPT-NPs, HA/10-HCPT-NPs, 10-HCPT-NPs, LIFU, 10-HCPT+LIFU, HA/CPPs-10-HCPT-NPs+LIFU, CPPs-10-HCPT-NPs+LIFU, HA/10-HCPT-NPs+LIFU, and 10-HCPT-NPs+LIFU (n=5). The control group received no treatment. 10-HCPT treatment groups received the same 10-HCPT dose of 4 mg 10-HCPT/kg corresponding to NPs. LIFU irradiation (1.0 MHz; 2.4 W/cm<sup>2</sup>; duty cycle, 50%; focal length, 1.5cm; pulse wave mode; 3 min) was undertaken after drug administration for 1 h [15]. Twenty-four hours after treatment, 10  $\mu$ L of CCK-8 reagent was added to each well and incubated for 1 h in an incubator. The optical density (OD) was read at 450 nm by a microplate reader. Cell survival rate was calculated using the following equation: Survival rate (%) =  $(As-Ab)/(Ac-Ab) \times 100\%$ , where as is the OD value in the experimental groups (culture medium containing cells, CCK-8 reagent, NPs). Ac is the OD value in the control group (culture medium containing cells, CCK-8 reagent, without NPs) and Ab is the OD value in the blank group (culture medium without cells and NPs, CCK-8 reagent).

### Apoptosis assay

SMMC-7721 cells in the exponential growth phase were digested and the cell concentration adjusted to  $5 \times 10^5$ /mL. Each well of six-well plates was seeded with 1 mL of the cell suspension, and then incubated at 37°C with 5% CO<sub>2</sub> in a humidified incubator for 24 h. To assess the effects of HA/CPPs-10-HCPT-NPs+LIFU irradiation on apoptosis, cells were divided into groups and treated as described above for the anti-proliferation assay. After overnight culture, cells were digested, centrifuged and collected. They were then washed thrice with cold PBS. Finally, cells were resuspended in 500  $\mu$ L of PBS and underwent flow cytometric analyses to test for apoptosis.

### In vivo targeting efficiency

To evaluate the distribution and tumor-targeting efficiency of HA/CPPs-10-HCPT-NPs in mice bearing the HCC xenograft, six mice were divided randomly into the HA/CPPs-10-HCPT-NPs group and CPPs-10-HCPT-NPs group. DiR-labeled NPs were injected *via* the tail vein. Real-time imaging was conducted by a small-animal *in vivo* fluorescence imaging system (IVIS Lumina III; PerkinElmer, Waltham, MA, USA). The distribution and intensity of

fluorescence signals *in vivo* were observed at 4 h and 24 h. After 24h, the mice were killed, and the tumor and organs extracted for additional *ex vivo* fluorescence imaging to assess the change in fluorescence intensity.

### In vivo ADV and ultrasound imaging

To verify further the targeting capability and effect of enhanced ultrasound imaging of HA/CPPs-10-HCPT-NPs *in vivo*, 15 mice bearing tumor xenografts were divided randomly into three groups: (1) HA/CPPs-10-HCPT-NPs+LIFU, (2) CPPs-10-HCPT-NPs+LIFU, (3) HA/CPPs-10-HCPT-NPs. Mice were injected with PFP-coated corresponding NPs *via* the tail vein. One hour after injection, the tumors of group (1) and group (2) were irradiated by LIFU (3.2 W/cm<sup>2</sup>; duty cycle, 50%; pulse wave mode; 2 min) [15]. An ultrasonic coupling agent was placed between the tumor surface and LIFU probe to ensure that the focus was in the tumor (focal length = 1.5cm). The linear array probe of the ultrasonic apparatus was used to scan tumor sites before and after LIFU irradiation. Ultrasonograms of tumor pre- and post-LIFU irradiation were observed to evaluate the enhanced ultrasound imaging of NPs irradiated by LIFU. The echo intensity of the images was calculated using an ultrasound image analyzer [15, 20].

### Therapeutic effect in vivo

To evaluate the anti-tumor therapeutic effect of combined application of HA/CPPs-10-HCPT-NPs with LIFU in mice bearing tumor xenografts, the tumor-bearing mice were distributed to 12 groups at random (n = 5): control, free 10-HCPT, HA/CPPs-10-HCPT-NPs, CPPs-10-HCPT-NPs, HA/10-HCPT-NPs, 10-HCPT-NPs, LIFU, 10-HCPT+LIFU, HA/CPPs-10-HCPT-NPs+LIFU, CPPs-10-HCPT-NPs+LIFU, HA/10-HCPT-NPs+LIFU, and 10-HCPT-NPs+LIFU. The control group received an injection of physiologic (0.9%) saline. The different formulations of 10-HCPT were injected at the same 10-HCPT dose of 4mg/kg body weight through the vena caudalis once every 2 days. 10-HCPT treatment started 20 days and ended 31 days after injection into SMMC-7721 cells. LIFU irradiation was carried out for 5 min at 1 h after injection of the 10-HCPT formulation. The LIFU probe was positioned directly above the tumor xenografts with the coupling medium. The LIFU parameters (3.2 W/cm<sup>2</sup>; duty cycle, 50%; focal length, 1.5 cm; pulse wave mode) were based on our previous study [15]. After 31 days, all mice were killed and tumor xenografts excised. The weight and size of tumor xenografts were measured and used to calculate tumor inhibition [42] and tumor volume. The

proliferation and apoptosis of tumor cells were assessed by immunohistochemical (IHC) staining with antibodies against proliferating cell nuclear antigen (PCNA) and the terminal deoxynucleotidyl transferase (TdT) dUTP nick-end labeling (TUNEL) assay, respectively. The proliferative index (PI) and apoptotic index (AI) were calculated according to the number of positively stained tumor cells divided by the total number of cells, which were counted from six randomly selected high-power fields. The histopathologic change of paraffin tissue section stained with hematoxylin and eosin (H&E) was also documented.

### Statistical analyses

Data are the mean  $\pm$  standard deviation, and were analyzed using SPSS 21.0 software (IBM, Armonk, NY, USA). One-way ANOVA and the Student's *t*-test were utilized for statistical evaluation. Differences were considered significant at  $P < 0.05$ .

## Results and Discussion

### Characterization of the NPs

NPs were punctiform in shape with good dispersity under optical microscopy (Figure 2A) and CLSM (Figure 2B) and showed a spherical morphology on TEM (Figure 2C). The mean particle size of CPPs-10-HCPT-NP and HA/CPPs-10-HCPT-NP was  $245.1 \pm 10.3$  nm and  $284.2 \pm 13.3$  nm (Figure

2D), and the mean zeta potential was  $45.50 \pm 2.09$  mV and  $-16.55 \pm 1.50$  mV (Figure 2E), respectively (Table 1). The surface potential of HA/CPPs-10-HCPT-NP formed after incubation of CPPs-10-HCPT-NP with HA solution was obviously negative. The change in the charge of NPs demonstrated that HA as an outer corona was introduced *via* electrostatic interaction. In addition, the Fourier transform infrared (FTIR) spectra also demonstrated successful modification by HA (Figure S1).

The UV-vis spectrum of HA/CPPs-10-HCPT-NPs ascertained that 10-HCPT was loaded successfully (Figure S2). The EE and LE of HA/CPPs-10-HCPT-NP were  $48.10\% \pm 3.13\%$  and  $5.23\% \pm 0.34\%$ , respectively.

**Table 1.** Particle size and zeta potential of HA/CPPs-10-HCPT-NPs and CPPs-10-HCPT-NPs.

| Nanoparticles      | Particle Size (nm) | Zeta Potential (mV) |
|--------------------|--------------------|---------------------|
| HA/CPPs-10-HCPT-NP | $284.23 \pm 13.28$ | $-16.55 \pm 1.50$   |
| CPPs-10-HCPT-NP    | $245.08 \pm 10.32$ | $45.50 \pm 2.09$    |

Values are the mean  $\pm$  SD (n = 3).

### In vitro ADV and ultrasound imaging of HA/CPPs-10-HCPT-NPs

PFP-coated NPs can be triggered to undergo a liquid-gas phase-transformation by external factors (e.g., ultrasound, temperature, lasers), but ultrasound

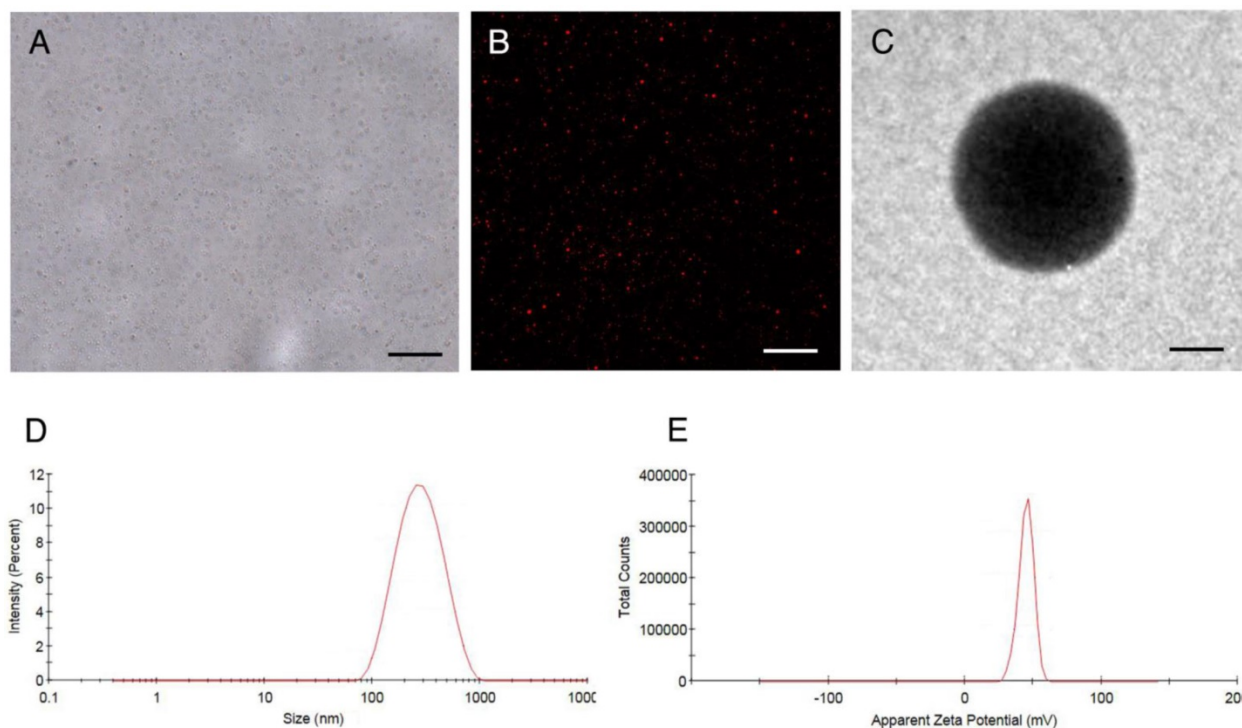


**Figure 2.** Characterization of HA/CPPs-10-HCPT-NPs. (A) optical microscopy image of HA/CPPs-10-HCPT-NPs, scale bar: 20  $\mu$ m. (B) CLSM image of Dil-stained HA/CPPs-10-HCPT-NPs, scale bar: 25  $\mu$ m. (C) TEM image of HA/CPPs-10-HCPT-NPs, scale bar: 100 nm. (D) Size distributions of HA/CPPs-10-HCPT-NPs. (E) Zeta potential of HA/CPPs-10-HCPT-NPs (n = 3).

is the best way to trigger ADV [50]. ADV denotes a transformation from liquid to gas when a liquid fluorocarbon reaches its phase-transformation threshold under irradiation with ultrasound energy [51]. In the ADV of HA/CPPs-10-HCPT-NPs triggered by LIFU *in vitro*, we investigated the influence of irradiation time and acoustic intensity on ADV. Before LIFU irradiation, a nanoemulsion of NPs in agar gel phantom showed low echo or no echo intensity (Figure 3A). Under B-mode ultrasound, the echo intensity of NPs increased with increasing time in the 2 W/cm<sup>2</sup> group. In the 2.4 W/cm<sup>2</sup> group, the echo intensity peak was at 3 min, and began to decline at 4 min. We speculated that some of the

phase-transformation NPs ruptured when their volume increased to a certain extent, and so the echo intensity of the NPs declined. In the 2.8 W/cm<sup>2</sup> group, though the echo intensity of the NPs increased with increasing time in the first 3 min, the echo intensity of the NPs began to decline at 4 min. Interestingly, the echo intensity was lower than that of the 2.4 W/cm<sup>2</sup> group at 3 min. A possible reason is that the acoustic intensity at 2.8 W/cm<sup>2</sup> at 3 min was sufficient to induce UTMD caused by LIFU, the phase-transformation NPs formed microbubbles, and then the microbubbles ruptured, and so the echo intensity was markedly reduced.

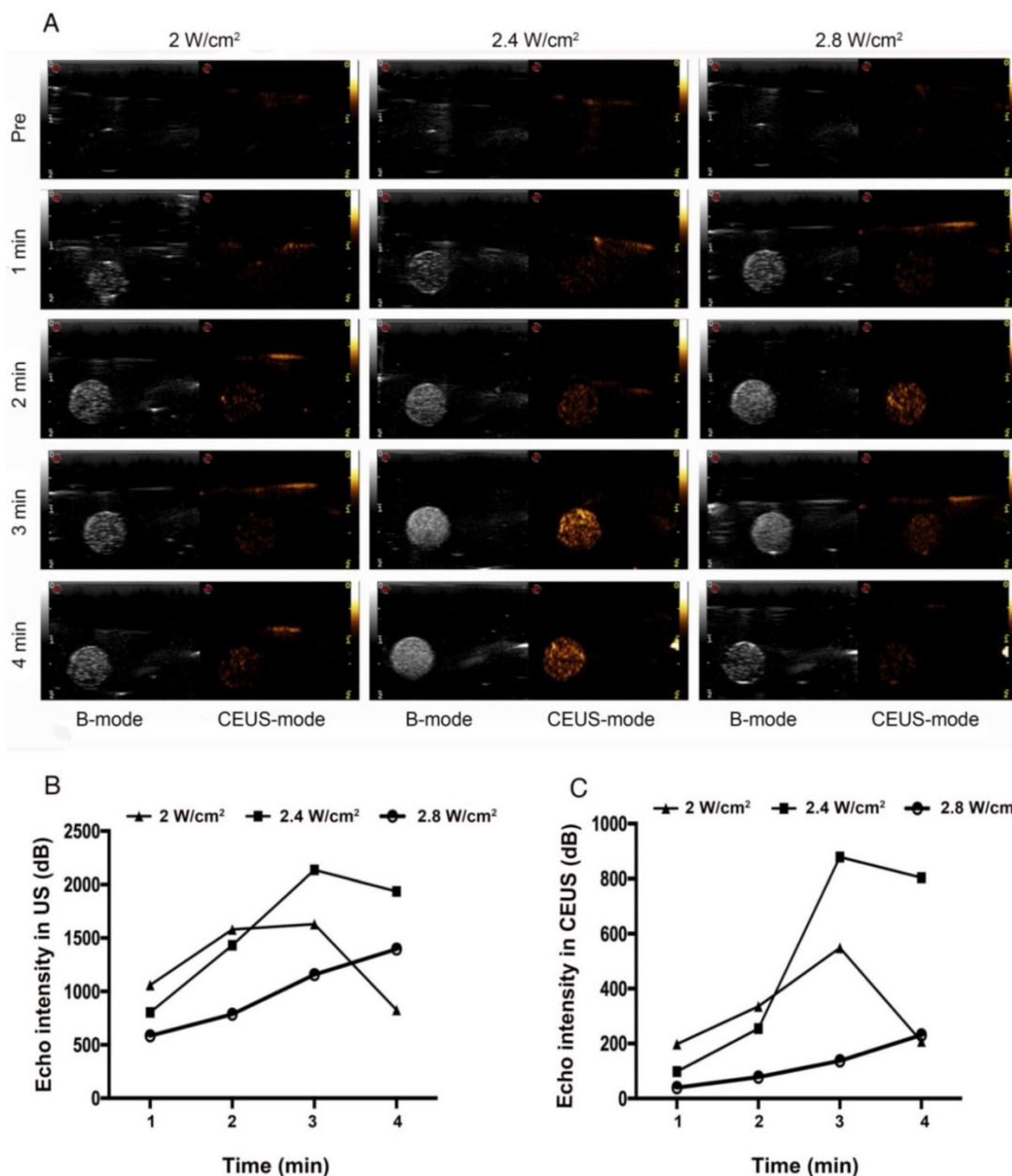


**Figure 3.** ADV and ultrasound imaging of HA/CPPs-10-HCPT-NPs with encapsulation of PFP *in vitro*. The time- and acoustic intensity-dependent ADV and ultrasound imaging of HA/CPPs-10-HCPT-NPs triggered by LIFU (left of each ultrasonogram: B-mode; right of each ultrasonogram: CEUS-mode) (A). Quantitative analyses of the echo intensity of NPs after different acoustic intensities and different times of LIFU irradiation in B-mode (B) and CEUS-mode (C).

Thus, the optimal condition of ADV generated by LIFU was 2.4 W/cm<sup>2</sup> at 3 min (Figure 3A, B). We could also draw the same conclusion from the CEUS mode (Figure 3A, C). Under LIFU irradiation, the echo intensity of HA/CPPs-10-HCPT-NPs without PFP in agar gel phantom did not change with the change of ultrasound intensity or time. Both in B-mode and CEUS mode, the nanoemulsion of NPs without PFP showed no echo (Figure S3). The results stated above demonstrated that a nanoemulsion containing NPs with encapsulated PFP generated a high echo signal at a certain intensity of ultrasound due to PFP causing ADV.

### Targeting efficiency of HA/CPPs-10-HCPT-NPs *in vitro*

To improve the efficiency of NPs targeting to tumors, a ligand-mediated active targeting strategy is regarded as the ideal choice [25]. HA has numerous excellent properties: non-toxicity, non-immunogenicity, and biodegradability, HA is also involved in the motility, matrix adhesion, and proliferation of cells [31]. The target-binding experiment of SMMC-7721 cells with HA/CPPs-10-HCPT-NPs or CPPs-10-HCPT-NPs showed many HA/CPPs-10-HCPT-NPs surrounding SMMC-7721 cells, and that some entered SMMC-7721 cells. These observations

suggested that HA/CPPs-10-HCPT-NPs could closely adhere to SMMC-7721 cells overexpressing CD44 (Figure S4A) and could penetrate cells through the cell membrane (Figure 4A). However, in the CPPs-10-HCPT-NP group, NPs rarely adhered to SMMC-7721 cells (Figure 4 B), which demonstrated that HA had an important role in helping NPs to target SMMC-7721 cells. The HA/CPPs-10-HCPT-NPs+HAase group had no or few NPs adhering to SMMC-7721 cells after HAase administration, which further demonstrated that HA was an important mediatory factor targeting HCC (Figure 4C). HA can bind to its receptors, such as CD44 and receptor for HA mediated motility (RHAMM), so HA has been used widely for the study of tumor-targeting drug-delivery systems [27]. HA is considered to be a “switch” coating on the surface of NPs *via* electrostatic interactions and protects NPs from plasma proteins to prolong the circulation of NPs. More importantly, HAase (an endo-glucosidase present extensively in weakly acidic tumor microenvironments) can hydrolyze HA, which “turns off” the protective function of HA, and simultaneously “turns on” the penetrating activity of CPPs-10-HCPT-NPs for improved uptake by tumor cells [27].

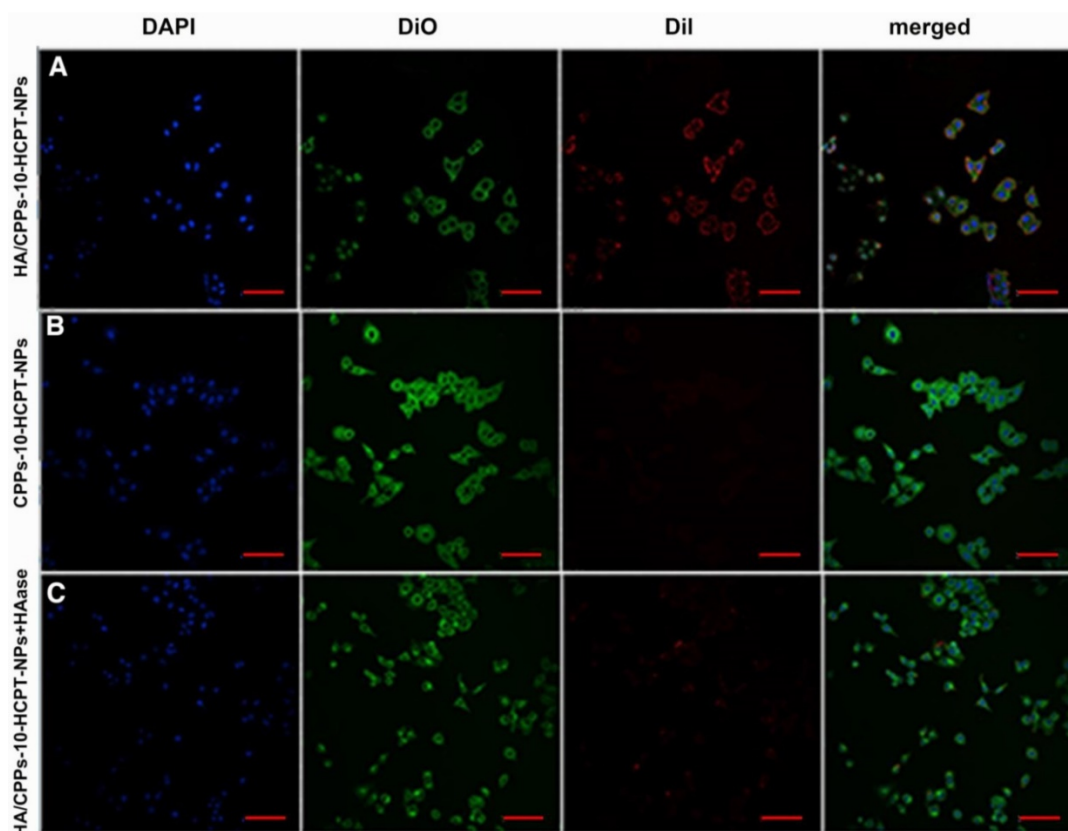


**Figure 4.** Efficiency of various NPs targeting SMMC-7721 cells *in vitro*. CLSM images of SMMC-7721 cells incubated with different NPs (scale bar: 100  $\mu$ m); blue: nuclei stained by DAPI; green: cell membrane stained by DiO; red: NPs stained by Dil; (A) HA/CPPs-10-HCPT-NPs group, (B) CPPs-10-HCPT-NPs group, (C) HA/CPPs-10-HCPT-NPs+HAase group.

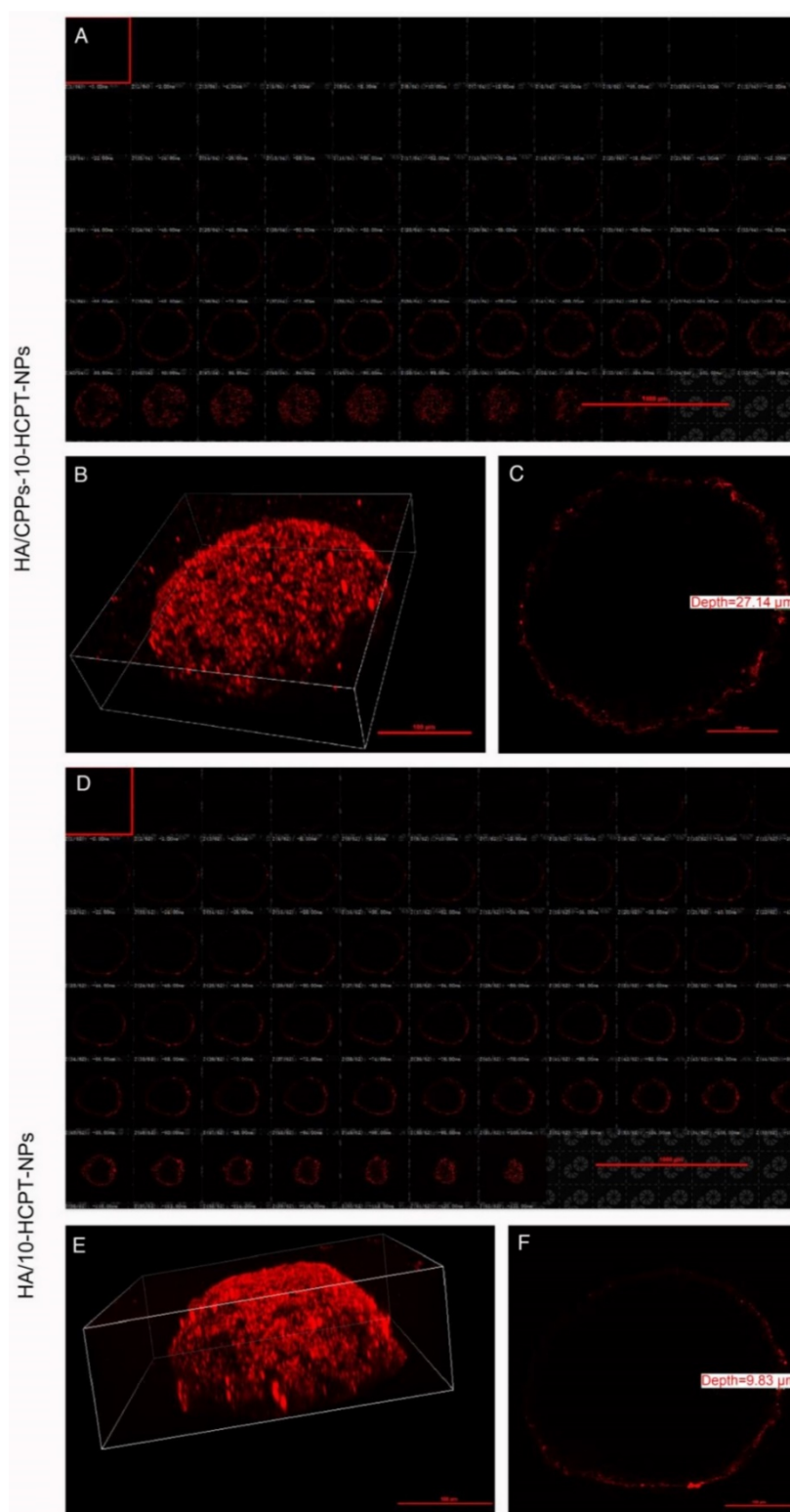


**Figure 5.** Penetration of Dil-stained NPs in SMMC-7721 cells using 3D MCTS. Multi-level scan of MCTS at 2 μm intervals showing the penetration of HA/CPPs-10-HCPT-NPs (A) and HA/10-HCPT-NPs without CPPs (D). 3D stereogram of MCTS in the HA/CPPs-10-HCPT-NPs group (B) and HA/10-HCPT-NPs group (E). Penetration depth of HA/CPPs-10-HCPT-NPs (C) and HA/10-HCPT-NPs (F).

### Penetration efficiency of HA/CPPs-10-HCPT-NPs *in vitro*

3D MCTS can better mimic the tumor microenvironment (such as heterogeneous tumor perfusion, high cell density, acidic pH, and increased

interstitial pressure) of solid tumors *in vivo* than monolayer tumor cells [52,53]. Thus, to determine the penetrating efficacy of HA/CPPs-10-HCPT-NPs, a 3D MCTS experiment with SMMC-7721 cells was undertaken. In the HA/CPPs-10-HCPT-NPs group,

the number of NPs clustered around the 3D MCTS and that had penetrated into the cell sphere was greater than that of the HA/10-HCPT-NPs group (Figure 5A, B, D, E), and the penetration depth was 27.14  $\mu\text{m}$  (Figure 5C). However, in the HA/10-HCPT-NPs without CPPs group, only a thin layer of NPs adhered to the 3D MCTS and penetrated into the 3D MCTS with a depth of only 9.83  $\mu\text{m}$  (Figure 5F), which was 2.76-fold thinner than that of the HA/CPPs-10-HCPT-NPs group. These results suggested that CG-TAT-GC markedly promoted the entry of NPs into 3D MCTS, and that HA/CPPs-10-HCPT-NPs could penetrate deeper into 3D MCTS than HA/10-HCPT-NPs. We hypothesized that HA/10-HCPT-NPs could not penetrate into the cells in a timely manner after binding to CD44 on the cell membrane. However, when CD44 on 3D MCTS was saturated with HA, no more NPs adhered to 3D MCTS. More importantly, cysteine-flanked CG-TAT-GC could induce HA/CPPs-10-HCPT-NPs to penetrate deeper into 3D MCTS than was observed in the control group [24].

### Anti-proliferation assay

The CCK-8 assay was used to analyze the anti-proliferation efficiency of a combination of HA/CPPs-10-HCPT-NPs with LIFU. The cytotoxicity of free 10-HCPT was higher than that of HA/CPPs-10-HCPT-NPs, CPPs-10-HCPT-NPs, HA/10-HCPT-NPs, or 10-HCPT-NPs, so cell survival in the free 10-HCPT group was lower than that of the other groups without LIFU (Figure 6). One reason for this result could be that 10-HCPT is more susceptible to passive diffusion, internalization, penetration, and entry into cells than NPs, whereas the 10-HCPT in NPs was released gradually into the plasma, and cytotoxicity increased with time [10]. There was no significant difference ( $P > 0.05$ ) between the control group and LIFU irradiation-only group in terms of survival, showing that the LIFU irradiation dose was safe for cells with no obvious toxicity. Cell survival in the 10-HCPT+LIFU irradiation group was lower than that of the free 10-HCPT group, which could be related to the increased permeability of cell membranes caused by LIFU irradiation, which facilitated 10-HCPT entry into cells [8, 28, 54]. More importantly, the cytotoxicity in the HA/CPPs-10-HCPT-NPs+LIFU group was higher than that of other NPs+LIFU groups. Cell survival in the HA/CPPs-10-HCPT-NPs+LIFU group was also the lowest of all groups. This finding was because guidance by the targeting function of HA, increased the number of HA/CPPs-10-HCPT-NPs surrounding SMMC-7721 cells compared to CPPs-10-HCPT-NPs without HA.

With the guidance of CG-TAT-GC, HA/CPPs-10-HCPT-NPs showed increased penetration, surrounded the cells, and could pass through the cell membrane into the cytoplasm and even into the nucleus to a greater extent than the HA/10-HCPT-NPs and 10-HCPT-NPs groups. In addition, under LIFU irradiation, the drug-loaded NPs surrounded SMMC-7721 cells and penetrated the cell membrane to enter cells to undergo ADV and then UTMD. This phenomenon promoted drug release from drug-loaded NPs and enhanced cell destruction. The microbubble-induced cavitation generated by LIFU markedly enhanced the tumor cell killing effect.

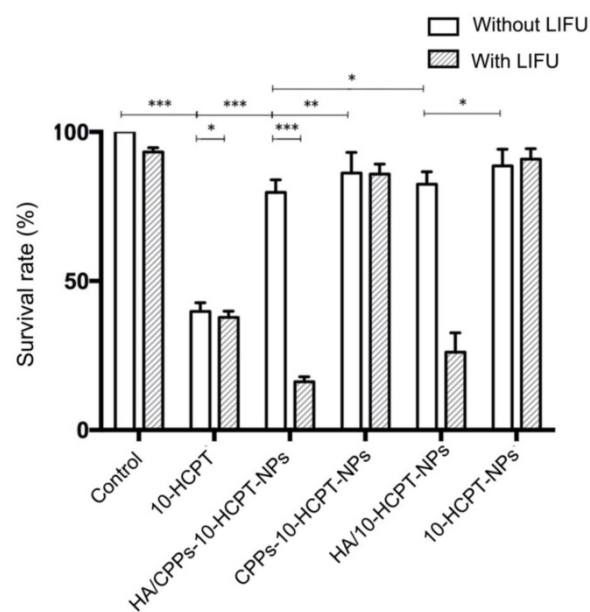


**Figure 6.** Anti-proliferation efficiency of NPs as determined by the CCK-8 assay.

### Apoptosis assay

To further study the synergistic efficiency of HA/CPPs-10-HCPT-NPs and LIFU, flow cytometry was undertaken to measure apoptosis. Apoptosis in the HA/CPPs-10-HCPT-NPs+LIFU group was the highest of all the groups (Figure 7A, B), suggesting that HA/CPPs-10-HCPT-NPs+LIFU had the best therapeutic efficiency in SMMC-7721 cells. Sustained release from the drug-loaded NPs [10] and the apoptosis percentages of the drug-loaded NPs groups (Figure 7A c-f) were lower than that of the free 10-HCPT group (Figure 7A b). However, when drug-loaded NPs were combined with LIFU irradiation, the apoptosis percentages in the drug-loaded NPs+LIFU groups (Figure 7A i-l) were higher than that of the free 10-HCPT+LIFU group, especially for HA/CPPs-10-HCPT-NPs+LIFU (Figure 7A i). We speculated that the main reasons were due to the targeting of HA and especially the penetrability of CG-TAT-GC (which promoted many NPs to

surround and gain entry into cells), the explosive force generated by the cavitation effect of UTMD, and increased local drug concentrations in tumor cells. Therefore, the cause of the increased apoptosis percentage was the synergistic effect of HA/CPPs-10-HCPT-NPs with LIFU, where the apoptosis percentage in the pure LIFU group (Figure 7A g) was not significant ( $P>0.05$ ) compared with that in the control group (Figure 7A a). These results were consistent with those from the anti-proliferation experiments.

### Targeting efficiency *in vivo*

Nude mice bearing SMMC-7721 cell tumor xenografts were administered (i.v.) 200  $\mu$ L of DiR-labeled CPPs-10-HCPT-NPs or HA/CPPs-10-HCPT-NPs (1 mg/kg) *via* the tail vein. The fluorescence signal at the tumor site in the targeted group was significantly higher than that in non-targeted group at predetermined time points (Figure 8A-D). We observed the fluorescence intensities of

tumors and organs *ex vivo* for the targeted group and the non-targeted group. The targeting and membrane-penetrating ability of the targeted group were better than those of the non-targeted group (Figure 8E, F). The fluorescence intensity of HA/CPPs-10-HCPT-NPs in the tumor location was much stronger than that of CPPs-10-HCPT-NPs at 4 h and 24 h after administration. This result was confirmed by *ex vivo* imaging of tumor nodes collected from mice bearing SMMC-7721 cell tumor xenografts 24 h after injection (Figure 8G). HA can bind specifically with CD44 overexpressed by HCC cells (Figure S4B, S5), so we speculated that the fluorescence signal in the non-targeted group was from the enhanced permeability and retention (EPR) effect, whereas the fluorescence signal at the tumor site in the targeted group was mainly from a synergy that was HA-mediated and CPPs-induced. The active targeting effect was significantly stronger ( $P<0.001$ ) than the EPR effect of passive targeting at the tumor site.

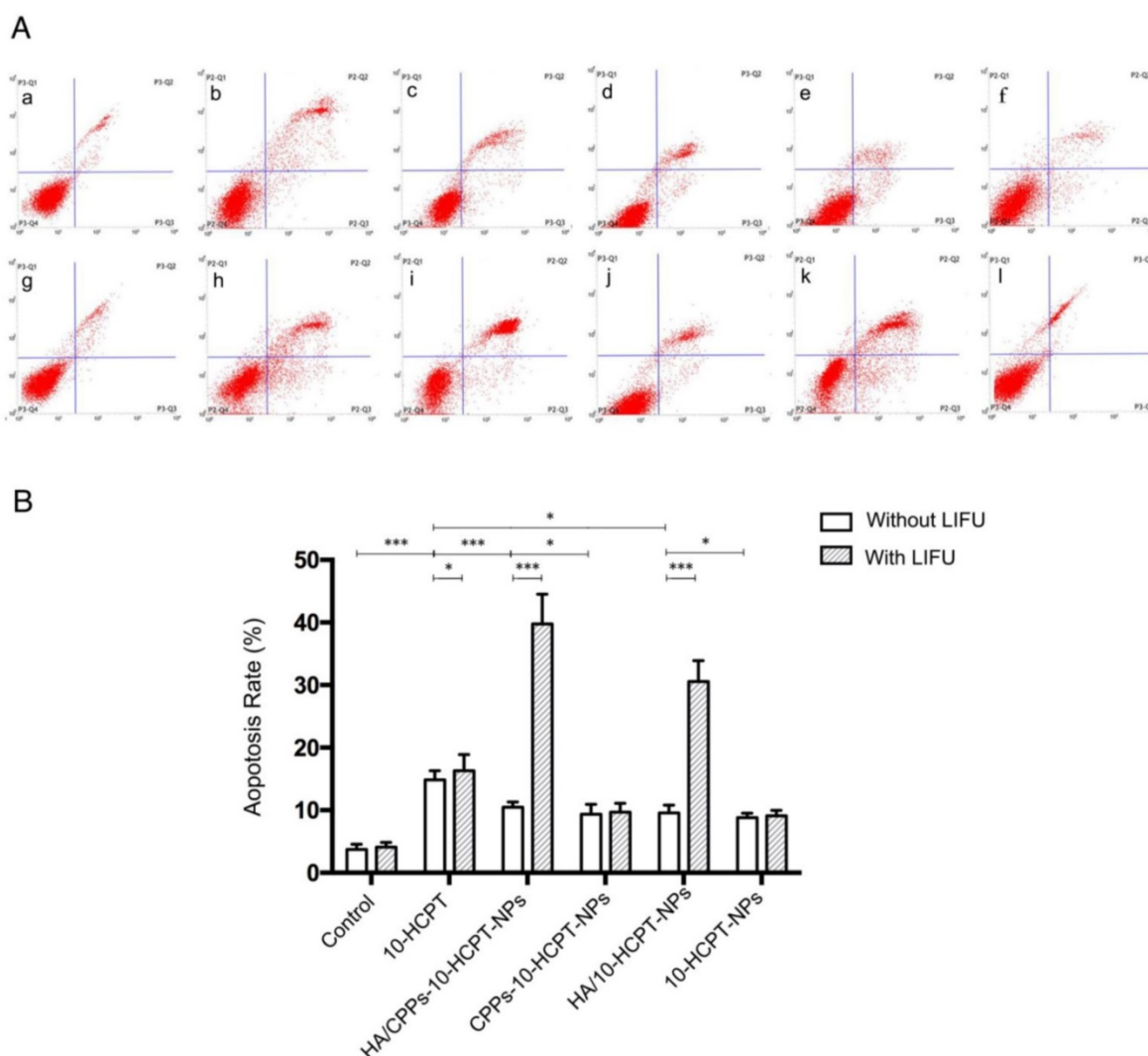


**Figure 7.** Apoptosis analyses by flow cytometry in groups of 10-HCPT. Normal cells without any treatment formed the control group (A a), free drug (A b), various NPs (A c-f) and those combined with LIFU (A g-l). Apoptosis rate in various groups (B).

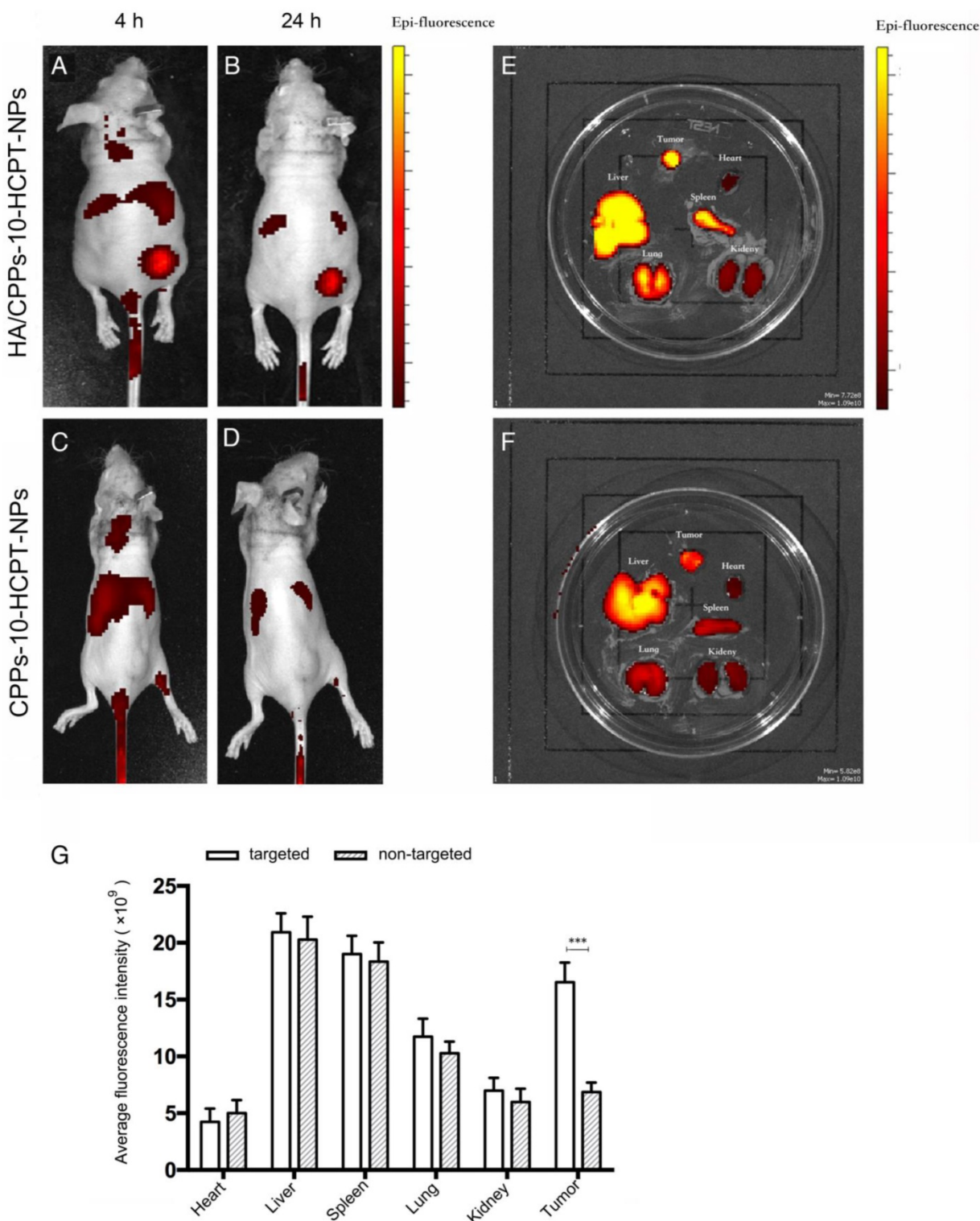


**Figure 8.** Real-time imaging of mice bearing SMMC-7721 tumors using a small-animal *in vivo* fluorescence imaging system. Imaging was carried out 4 h and 24 h after administration of HA/CPPs-10-HCPT-NPs (A, B) or CPPs-10-HCPT-NPs (C, D). *Ex vivo* fluorescence imaging of dissected organs 24 h after administration in the HA/CPPs-10-HCPT-NPs group (E) and CPPs-10-HCPT-NPs group (F). Mean fluorescence intensities of heart, liver, spleen, lung, kidney and tumors 24 h after administration of HA/CPPs-10-HCPT-NPs or CPPs-10-HCPT-NPs, \*\*\*P<0.001 (G).

**ADV and ultrasound imaging *in vivo***

When they reach the lesion site and ADV is triggered by LIFU, phase-transformation NPs can be used to enhance ultrasound imaging and to diagnose

diseases. Before injection of NPs, the ultrasonograms of tumors in each group showed a regular low echo (Figure 9A-C). One hour after injection *via* the tail vein, LIFU was undertaken in the HA/CPPs-10-HCPT-NPs+LIFU group and CPPs-10-HCPT-NPs+

LIFU group, and then B-mode and CEUS-mode imaging were used to observe the tumor sites. In the HA/CPPs-10-HCPT-NPs+LIFU group, the focal spot in the tumor showed a strong echo signal after LIFU irradiation (Figure 9D), whereas no obvious ultrasound enhancement was observed in the whole tumor site in the CPPs-10-HCPT-NPs+LIFU group (Figure 9E). These data demonstrated that HA/CPPs-10-HCPT-NPs could target tumor tissue actively, penetrate cell membranes to enter cells near the blood vessel and extracellular matrix deep into tumor cells far from the blood vessel, undergo ADV triggered by LIFU, and enhance ultrasound imaging. Conversely, CPPs-10-HCPT-NPs could not accumulate in the tumor location, insufficient ADV occurred, and a high echo signal was not obtained. A high echo signal was also not observed in the HA/CPPs-10-HCPT-NPs without LIFU group (Figure 9F), suggesting that PFP-loaded NPs could not initiate ADV by themselves *in vivo*. This result indicated indirectly that HA/CPPs-10-HCPT-NPs can experience ADV *in vivo* after triggering by LIFU, not temperature. These data were consistent with previous studies [15]. Analyses of ultrasound intensity showed that the echo intensity was markedly stronger after LIFU irradiation than before LIFU irradiation in the HA/CPPs-10-HCPT-NPs+LIFU group. In B-mode (Figure 9G) and CEUS-mode (Figure 9H), the increase in echo intensity in the HA/CPPs-10-HCPT-NPs+LIFU group was the highest of all the groups.

### Therapeutic effect of a combination of NPs with LIFU irradiation *in vivo*

We measured some indices to evaluate the therapeutic effect of combined application of HA/CPPs-10-HCPT-NPs with LIFU irradiation in mice bearing tumor xenografts. The combined effect of HA/CPPs-10-HCPT-NPs and LIFU inhibited tumor growth significantly (Figure 10A). Compared with other groups, tumor volume and tumor weight in the HA/CPPs-10-HCPT-NPs+LIFU group were the smallest (Figure 10B, Table 2) and inhibition percentage was the highest in all groups ( $P < 0.001$ ) (Table 2). There was no significant difference between the LIFU group and blank control group ( $P > 0.05$ ), suggesting that the dose of LIFU irradiation was safe. The antitumor effect of the free 10-HCPT group *in vivo* was inferior to that of other NPs groups. This result was different from the *in vitro* result. One reason may be that free 10-HCPT was metabolized quickly and 10-HCPT-loaded NPs had sustained release *in vivo*. In addition, the toxicity of 10-HCPT in drug-loaded NPs decreased and stability increased, which improved the anti-tumor effect [10, 38–41]. Similarly, the

antitumor effect in the HA/CPPs-10-HCPT-NPs group was stronger than that of the CPPs-10-HCPT-NPs group ( $P < 0.05$ ). The anti-tumor effect in the HA/10-HCPT-NPs group was also stronger than that of the 10-HCPT-NPs group because more targeted NPs (under HA mediation) can accumulate at the tumor site to release the drug. In addition, the antitumor effect of HA/CPPs-10-HCPT-NPs was better than that of HA/10-HCPT-NPs ( $P < 0.05$ ). We speculated that under CG-TAT-GC-mediation, more CPPs-modified NPs penetrated into cells through the cell membrane and killed tumor tissue cells directly. With better properties than previously reported ultrasound molecular probes, CG-TAT-GC-mediated NPs penetrated the extracellular matrix and cell membrane in sequence to reach the tumor site, which realized NPs targeting to more and deeper cells and inhibited tumor growth more precisely. Interestingly, the inhibition percentage for tumors in the HA/CPPs-10-HCPT-NPs+LIFU group was 1.16-fold ( $P < 0.05$ ) higher than that of the HA/CPPs-10-HCPT-NPs without LIFU group (Table 2), suggesting that the cavitation effect of HA/CPPs-10-HCPT-NPs triggered by LIFU played an important part in enhancing the anti tumor therapy [55–57].

**Table 2.** Mean tumor weight and mean percentage tumor inhibition in each group after treatment for 10 days (mean $\pm$ SD, n = 5).

| Group                    | Tumor weight (mg)         | Mean tumor inhibition rate (%) |
|--------------------------|---------------------------|--------------------------------|
| Saline control           | 2.15 $\pm$ 0.32           | -                              |
| Saline +LIFU             | 2.09 $\pm$ 0.30           | 2.59                           |
| 10-HCPT                  | 1.52 $\pm$ 0.19*#         | 29.17                          |
| 10-HCPT+LIFU             | 1.17 $\pm$ 0.18           | 45.51                          |
| HA/CPPs-10-HCPT-NPs      | 0.35 $\pm$ 0.06*          | 83.97                          |
| HA/CPPs-10-HCPT-NPs+LIFU | 0.05 $\pm$ 0.01*#         | 97.61                          |
| CPPs-10-HCPT-NPs         | 0.69 $\pm$ 0.11*#         | 67.99                          |
| CPPs-10-HCPT-NPs+LIFU    | 0.28 $\pm$ 0.02           | 86.7                           |
| HA/10-HCPT-NPs           | 0.46 $\pm$ 0.08*#         | 78.65                          |
| HA/10-HCPT-NPs+LIFU      | 0.11 $\pm$ 0.02           | 94.97                          |
| 10-HCPT-NPs              | 0.77 $\pm$ 0.13* $\Delta$ | 64.21                          |
| 10-HCPT-NPs+LIFU         | 0.34 $\pm$ 0.04           | 83.92                          |

\* $P < 0.05$  vs Saline control group;

# $P < 0.05$  vs HA/CPPs-10-HCPT-NPs group;

$\Delta P < 0.05$  vs HA/10-HCPT-NPs group.

As a new ultrasound molecular imaging and treatment system developed by our research team, LIFU is being used increasingly in ultrasound molecular imaging, targeted drug delivery, and antitumor research [15, 42]. Using low-power ultrasound irradiation and avoiding damage to surrounding normal tissues, LIFU can simultaneously focus on the tumor site and trigger drug release accurately.

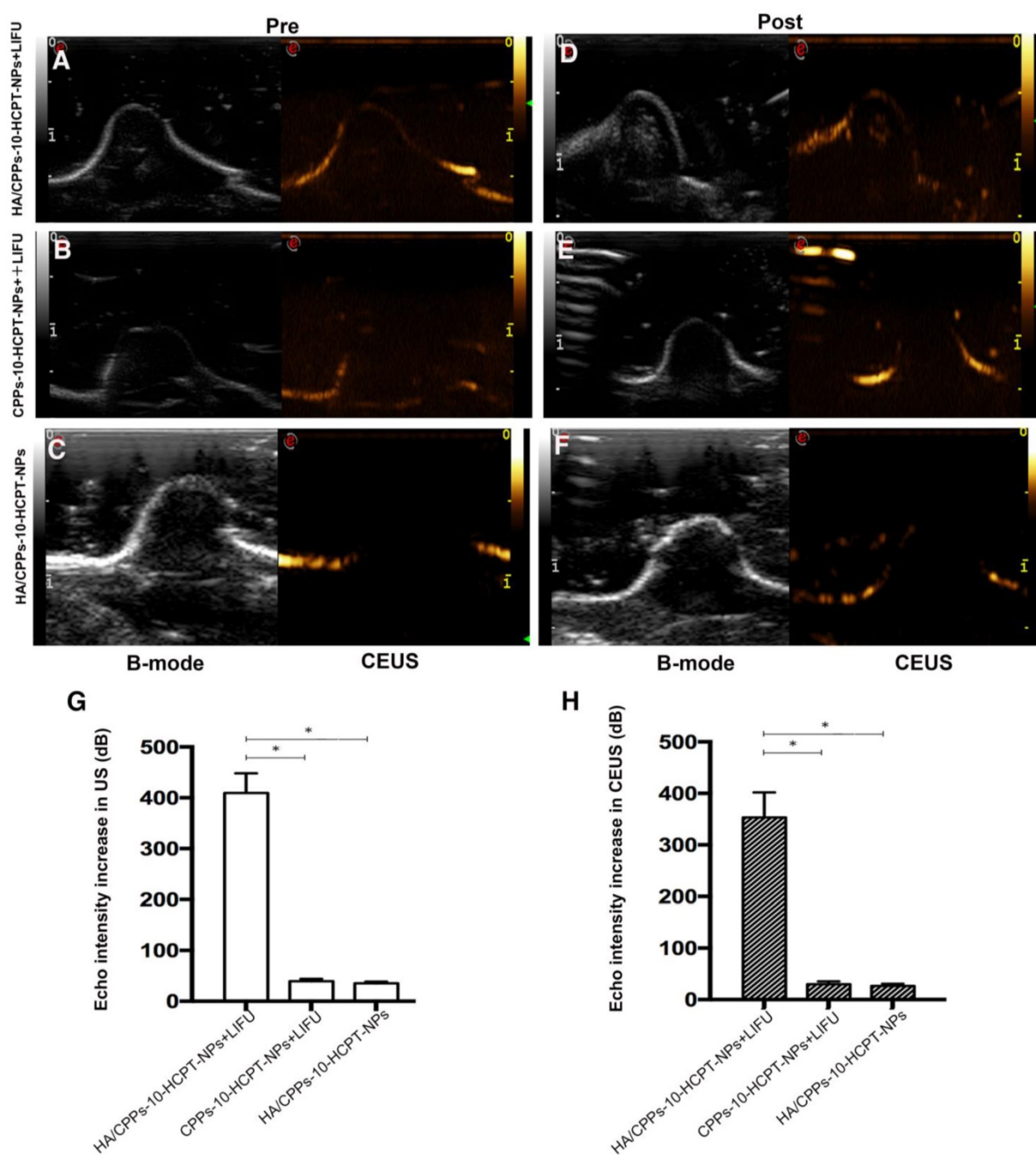


**Figure 9.** Ultrasound imaging of NPs observing ADV before and after LIFU irradiation in tumor sites. Ultrasound imaging of mice-bearing tumors before and after LIFU irradiation in the HA/CPPs-10-HCPT-NPs+LIFU group (A, D), CPPs-10-HCPT-NPs+LIFU group (B, E) and HA/CPPs-10-HCPT-NPs group (C, F). B-mode is on the left and CEUS-mode is on the right. Echo intensity increased in B-mode (G) and CEUS-mode (H) imaging of tumors in each group.

In the control group and LIFU group, H&E staining of tumor tissue showed normal cell morphology, whereas the largest number of lysed cell membranes and nuclear fragmentation were observed in the HA/CPPs-10-HCPT-NPs+LIFU group (Figure 11A). The TUNEL assay was used to evaluate apoptosis in tissue sections (apoptotic cell nuclei were stained brown (Figure 11B)) and the AI was calculated (Figure 11D). The most significant apoptosis occurred in the HA/CPPs-10-HCPT-NPs+LIFU group ( $P < 0.05$ ). PCNA-positive cell nuclei were also stained brown (Figure 11C). The PI in the HA/CPPs-10-HCPT-NPs+

LIFU group was the lowest of all groups ( $P < 0.05$ ) (Figure 11E). These results were consistent with H&E staining. Hence, the most effective treatment group was HA/CPPs-10-HCPT-NPs+LIFU group because PFP-coated CPPs-modified targeted drug-loaded NPs underwent ADV triggered by LIFU irradiation. This phenomenon, along with ultrasonic cavitation, mechanical effects and drug release, increased the effect of treatment. Thus, the combined application of HA/CPPs-10-HCPT-NPs with LIFU irradiation improved the therapeutic efficacy of HCC xenografts in nude mice dramatically.

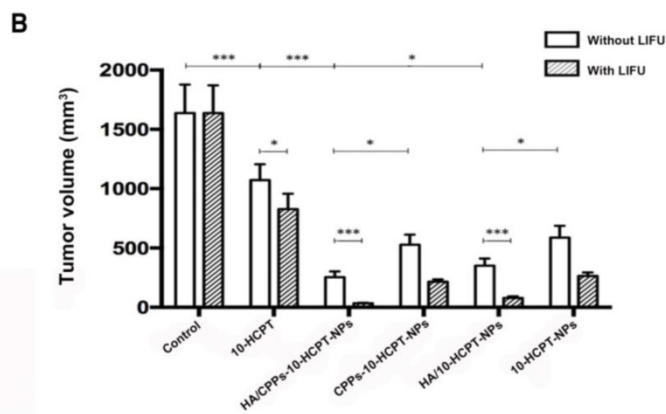
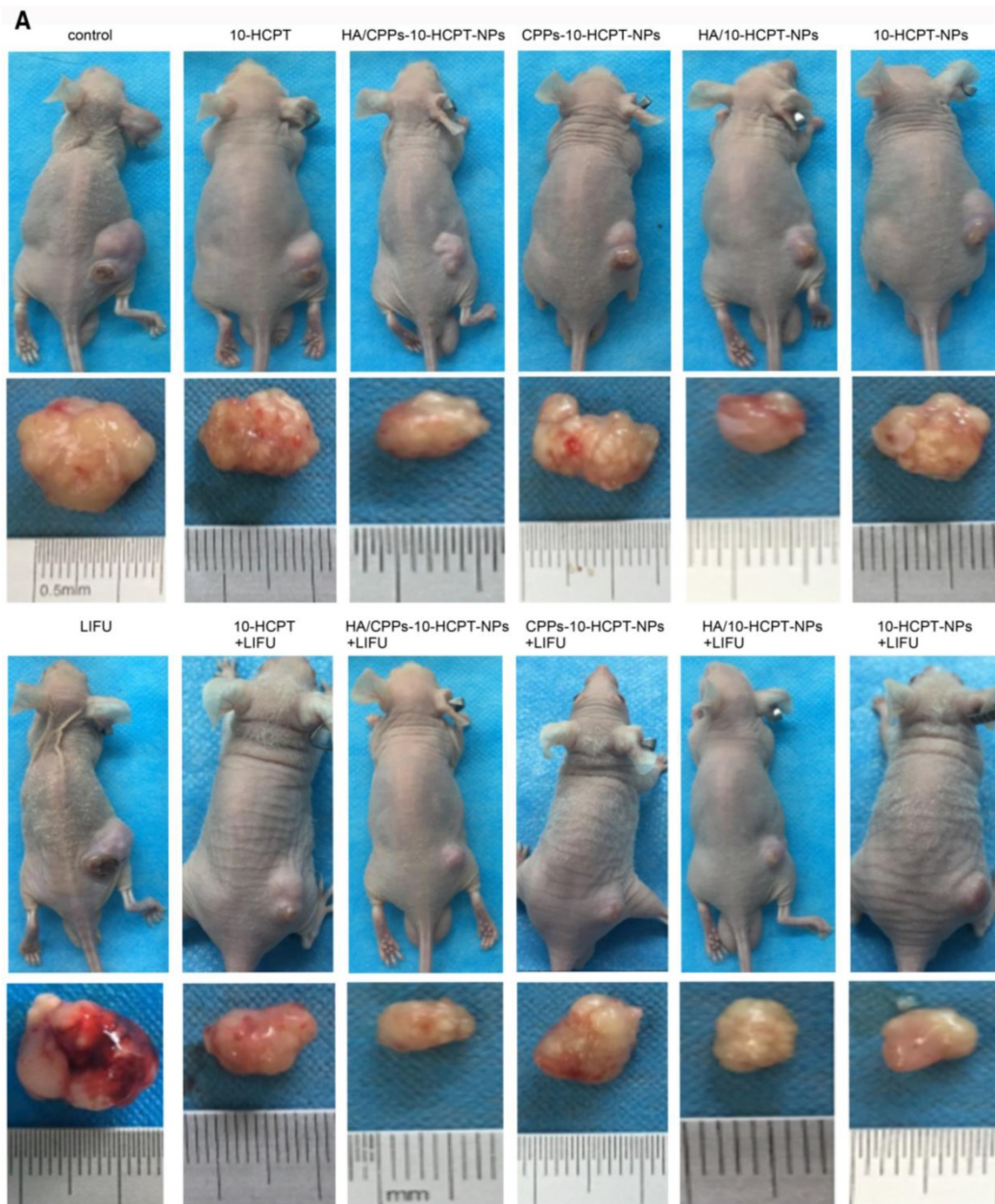


**Figure 10.** Mice bearing SMMC-7721 tumor xenografts and tumor specimens at the end of different treatments (A). Mean tumor volumes at the end of the treatment in various groups (B).

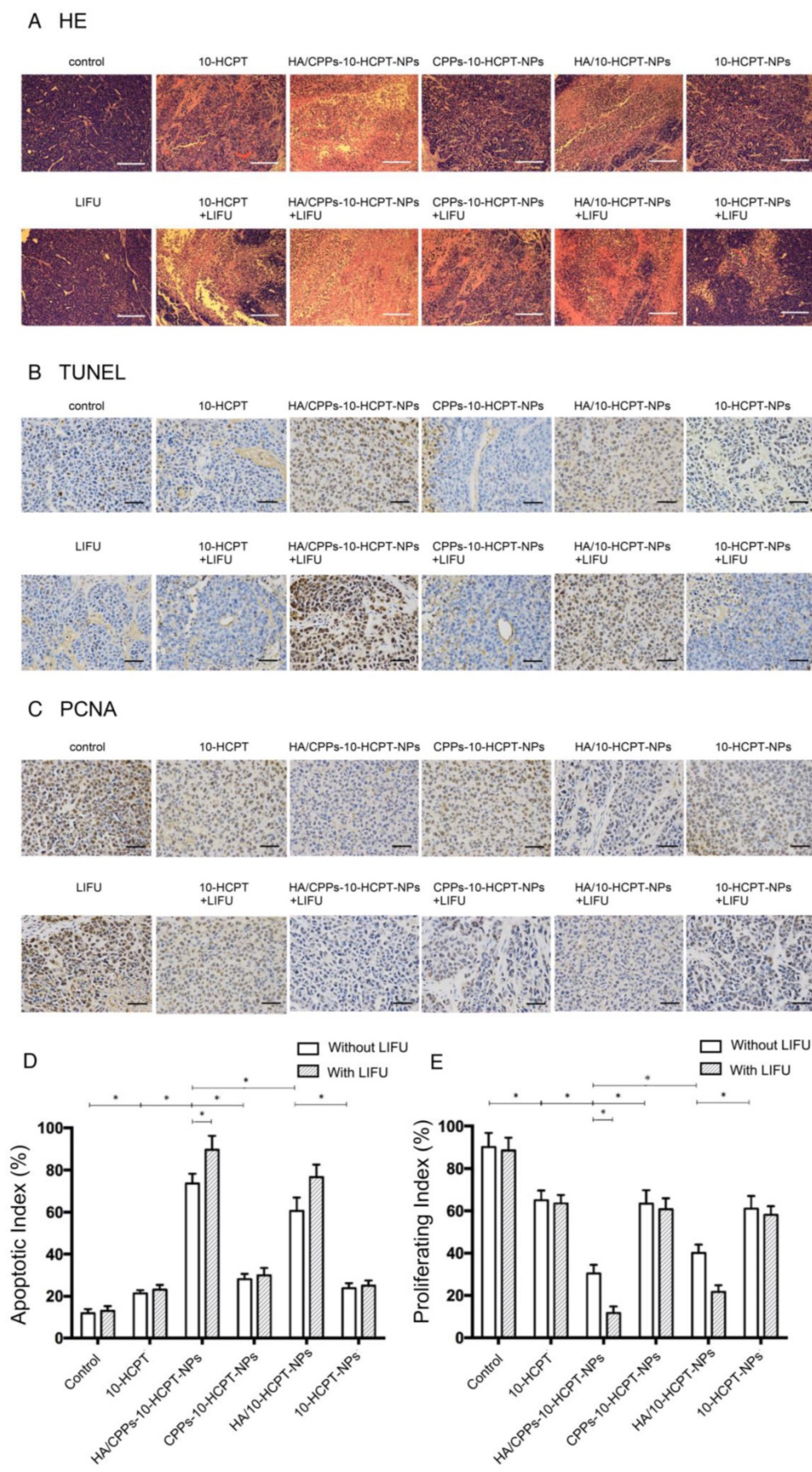


**Figure 11.** Anti-tumor efficacy observed by pathological examination of xenograft tissue in various groups. (A) Histologic changes of tumor tissues by H&E staining (magnification, 100 $\times$ ; scale bar: 200  $\mu$ m), microscopy images of expression of TUNEL (magnification, 400 $\times$ ; scale bar: 50  $\mu$ m) (B) and PCNA (magnification, 400 $\times$ ; scale bar: 50  $\mu$ m) (C), proliferative index (D) and apoptosis index (E) of tumor tissues in various groups.

## Conclusions

We prepared HA/CPPs-10-HCPT-NPs successfully. These agents have three main advantages. First, HA/CPPs-10-HCPT-NPs can target and accumulate in HCC cells actively (with HA) and passively (EPR effect). Second, induced by CG-TAT-GC, HA/CPPs-10-HCPT-NPs can penetrate the extracellular matrix, cellular membrane and even into the nucleus. Third, HA/CPPs-10-HCPT-NPs in and near HCC cells can undergo ADV and then UTMD triggered by LIFU. This enhances tumor-site imaging, improves drug release, increases intracellular “explosive effects” caused by ultrasound cavitation and mechanical effects to realize “real” cell-level imaging and intracellular physicochemical synergistic treatment of tumors. Our developed NPs can realize real ultrasound molecular imaging at the cellular level. Under LIFU irradiation, it also realizes precise theranostics at an early stage. Hence, HA/CPPs-10-HCPT-NPs+LIFU is a new strategy that integrates the diagnosis and treatment of HCC.

## Abbreviations

LIFU: low-intensity focused ultrasound; HCC: hepatocellular carcinoma; ADV: acoustic droplet vaporization; CLSM: confocal laser scanning microscopy; 3D: three-dimensional; MCTS: multicellular tumor spheroid; FCM: flow cytometry; H & E: hematoxylin and eosin; PCNA: proliferating cell nuclear antigen; TUNEL: terminal deoxynucleotidyl transferase (TdT) dUTP nick-end labeling; NPs: nanoparticles; PI: proliferative index; AI: apoptotic index; PFP: perfluoropentane; CPPs: cell-penetrating peptides; HIV-1 TAT: human immunodeficiency virus type-1 transactivating transcriptional activator; CD: cluster of differentiation; HA: hyaluronic acid; HAase: hyaluronidase; 10-HCPT: 10-hydroxy camptothecin; UTMD: ultrasound-targeted microbubble destruction; DPPC: 1,2-Dipalmitoyl-sn-glycero-3-phosphatidylcholine; DC-Chol: 3-(N-(N',N'-Dimethylaminoethane) carbamoyl) cholesterol; DiI: 1,1'-Diiododecyl-3,3,3',3'-tetramethylindocarbocyanine perchlorate; DiO: 3,3'-diiododecylcarbocyanine perchlorate; DAPI: 4', 6-diamidino-2-phenylindole; DiR: 1,1'-Diiododecyl-3,3,3',3'-tetramethylindocarbocyanine iodide; DMEM: Dulbecco's modified Eagle's medium; FBS: fetal bovine serum; CCK-8: cell counting Kit 8; TEM: transmission electron microscope; PBS: phosphate-buffered saline; HPLC: high-performance liquid chromatography; CEUS: contrast-enhanced ultrasound; OD: optical density; IHC: immunohistochemical; FTIR: Fourier transform infrared; EPR: enhanced permeability and retention.

## Acknowledgements

This study was supported by National Natural Science Foundation of China (61471074, 81227801, 81471675, 81371578, 81630047, 31630026), Fundamental and Frontier Research Program of Chongqing (cstc2014jcyjA10031, cstc2014jcyjA10096) and College Program of Excellent Young Talents (2016, number 20).

## Supplementary Material

Supplementary figures and tables.

<http://www.thno.org/v08p1892s1.pdf>

## Competing Interests

The authors have declared that no competing interest exists.

## References

- Pariikh S, Hyman D. Hepatocellular cancer: a guide for the internist. *Am J Med.* 2007; 120: 194-202.
- Fornier A, Llovet JM, Bruix J. Hepatocellular carcinoma. *Lancet.* 2012; 379: 1245-55.
- Torre LA, Bray F, Siegel RL, et al. Global cancer statistics, 2012. *CA Cancer J Clin.* 2015; 65: 87-108.
- Yang T, Zhao PX, Rong Z, et al. Anti-tumor efficiency of lipid-coated cisplatin nanoparticles co-loaded with microRNA-375. *Theranostics.* 2016; 6: 142-54.
- Ma L, Li GX, Zhu HQ, et al. 2-Methoxyestradiol synergizes with sorafenib to suppress hepatocellular carcinoma by simultaneously dysregulating hypoxia-inducible factor-1 and -2. *Cancer Lett.* 2014; 355: 96-105.
- Guvener N, Appold L, de Lorenzi F, et al. Recent advances in ultrasound-based diagnosis and therapy with micro- and nanometer-sized formulations. *Methods.* 2017; 130: 4-13.
- Senior R, Becher H, Monaghan M, et al. Contrast echocardiography: evidence-based recommendations by European Association of Echocardiography. *Eur J Echocardiogr.* 2009; 10: 194-212.
- Hernot S, Klibanov AL. Microbubbles in ultrasound-triggered drug and gene delivery. *Adv Drug Deliv Rev.* 2008; 60: 1153-66.
- Youk JH, Kim CS, Lee JM. Contrast-enhanced agent detection imaging: value in the characterization of focal hepatic lesions. *J Ultrasound Med.* 2003; 22: 897-910.
- Xing LX, Shi QS, Zheng KL, et al. Ultrasound-Mediated Microbubble Destruction (UMMD) Facilitates the Delivery of CA19-9 Targeted and Paclitaxel Loaded mPEG-PLGA-PLL Nanoparticles in Pancreatic Cancer. *Theranostics.* 2016; 6: 1573-87.
- Zhou Y, Gu HT, Xu Y, et al. Targeted antiangiogenesis gene therapy using targeted cationic microbubbles conjugated with CD105 antibody compared with untargeted cationic and neutral microbubbles. *Theranostics.* 2015; 5: 399-417.
- Mozafari M, Shimoda M, Urbanska AM, et al. Ultrasound-targeted microbubble destruction: toward a new strategy for diabetes treatment. *Drug Discov Today.* 2016; 21: 540-3.
- Hobbs SK, Monsky WL, Yuan F, et al. Regulation of transport pathways in tumor vessels: role of tumor type and microenvironment. *Proc Natl Acad Sci U S A.* 1998; 95: 4607-12.
- Min HS, You DG, Son S, et al. Echogenic Glycol Chitosan Nanoparticles for Ultrasound-Triggered Cancer Theranostics. *Theranostics.* 2015; 5: 1402-18.
- Liu JX, Shang TT, Wang FJ, et al. Low-intensity focused ultrasound (LIFU)-induced acoustic droplet vaporization in phase-transition perfluoropentane nanodroplets modified by folate for ultrasound molecular imaging. *Int J Nanomedicine.* 2017; 12: 911-23.
- Li H, Wang JH, Wang P, et al. Phase-transition contrast nanocapsules triggered by low-intensity ultrasound. *Chem Commun (Camb).* 2014; 50: 15163-6.
- You YF, Wang ZG, Ran HT, et al. Nanoparticle-enhanced synergistic HIFU ablation and transarterial chemoembolization for efficient cancer therapy. *Nanoscale.* 2016; 8: 4324-39.
- Torchilin VP, Levchenko IS, Rammohan R, et al. Cell transfection in vitro and in vivo with nontoxic TAT peptide-liposome-DNA complexes. *Proc Natl Acad Sci U S A.* 2003; 100: 1972-7.
- Liu ZH, Li MY, Cui DF, et al. Macro-branched cell-penetrating peptide design for gene delivery. *J Control Release.* 2005; 102: 699-710.
- Ren JL, Xu CS, Zhou ZY, et al. A novel ultrasound microbubble carrying gene and Tat peptide: preparation and characterization. *Acad Radiol.* 2009; 16: 1457-65.

21. Patel SS, Belmont BJ, Sante JM, et al. Natively unfolded nucleoporins gate protein diffusion across the nuclear pore complex. *Cell*. 2007; 129: 83-96.
22. Yamano S, Viet CT, Dang D, et al. Ex vivo nonviral gene delivery of mu-opioid receptor to attenuate cancer-induced pain. *Pain*. 2017; 158: 240-51.
23. Zhou ZY, Zhang P, Ren JL, et al. Synergistic effects of ultrasound-targeted microbubble destruction and TAT peptide on gene transfection: an experimental study in vitro and in vivo. *J Control Release*. 2013; 170: 437-44.
24. Siprashvili Z, Scholl FA, Oliver SF, et al. Gene transfer via reversible plasmid condensation with cysteine-flanked, internally spaced arginine-rich peptides. *Hum Gene Ther*. 2003; 14: 1225-33.
25. Zhang K, Li P, He YP, et al. Synergistic retention strategy of RGD active targeting and radiofrequency-enhanced permeability for intensified RF & chemotherapy synergistic tumor treatment. *Biomaterials*. 2016; 99: 34-46.
26. Zhang K, Xu HX, Jia XQ, et al. Ultrasound-Triggered Nitric Oxide Release Platform Based on Energy Transformation for Targeted Inhibition of Pancreatic Tumor. *ACS Nano*. 2016; 10: 10816-10828.
27. Jiang TY, Zhang ZH, Zhang YL, et al. Dual-functional liposomes based on pH-responsive cell-penetrating peptide and hyaluronic acid for tumor-targeted anticancer drug delivery. *Biomaterials*. 2012; 33: 9246-58.
28. Zhao YZ, Tian XQ, Zhang M, et al. Functional and pathological improvements of the hearts in diabetes model by the combined therapy of bFGF-loaded nanoparticles with ultrasound-targeted microbubble destruction. *J Control Release*. 2014; 186: 22-31.
29. Mattheolabakis G, Milane L, Singh A, et al. Hyaluronic acid targeting of CD44 for cancer therapy: from receptor biology to nanomedicine. *J Drug Target*. 2015; 23: 605-18.
30. Misra S, Heldin P, Hascall VC, et al. Hyaluronan-CD44 interactions as potential targets for cancer therapy. *Febs J*. 2011; 278: 1429-43.
31. Girish KS, Kemparaju K. The magic glue hyaluronan and its eraser hyaluronidase: a biological overview. *Life Sci*. 2007; 80: 1921-43.
32. Stern R. Hyaluronidases in cancer biology. *Semin Cancer Biol*. 2008; 18: 275-80.
33. Du JZ, Mao CQ, Yuan YY, et al. Tumor extracellular acidity-activated nanoparticles as drug delivery systems for enhanced cancer therapy. *Biotechnol Adv*. 2014; 32: 789-803.
34. Muthu MS, Leong DT, Mei L, et al. Nanotheranostics - application and further development of nanomedicine strategies for advanced theranostics. *Theranostics*. 2014; 4: 660-77.
35. Zhou YY, Du YZ, Wang L, et al. Preparation and pharmacodynamics of stearic acid and poly (lactic-co-glycolic acid) grafted chitosan oligosaccharide micelles for 10-hydroxycamptothecin. *Int J Pharm*. 2010; 393: 143-51.
36. Zhu ZS, Li Y, Li XL, et al. Paclitaxel-loaded poly(N-vinylpyrrolidone)-b-poly(epsilon-caprolactone) nanoparticles: preparation and antitumor activity in vivo. *J Control Release*. 2010; 142: 438-46.
37. Han SS, Li ZY, Zhu JY, et al. Dual-pH Sensitive Charge-Reversal Polypeptide Micelles for Tumor-Triggered Targeting Uptake and Nuclear Drug Delivery. *Small*. 2015; 11: 2543-54.
38. Li P, Zheng YY, Ran HT, et al. Ultrasound triggered drug release from 10-hydroxycamptothecin-loaded phospholipid microbubbles for targeted tumor therapy in mice. *J Control Release*. 2012; 162: 349-54.
39. Zhang LY, Yang M, Wang Q, et al. 10-Hydroxycamptothecin loaded nanoparticles: preparation and antitumor activity in mice. *J Control Release*. 2007; 119: 153-62.
40. Wang AX, Li S. Hydroxycamptothecin-loaded nanoparticles enhance target drug delivery and anticancer effect. *BMC Biotechnol*. 2008; 8: 46.
41. Hong MH, Zhu SJ, Jiang YY, et al. Efficient tumor targeting of hydroxycamptothecin loaded PEGylated niosomes modified with transferrin. *J Control Release*. 2009; 133: 96-102.
42. Gong YP, Wang ZG, Dong GF, et al. Low-intensity focused ultrasound mediated localized drug delivery for liver tumors in rabbits. *Drug Deliv*. 2016; 23: 2280-89.
43. Wang G, Zhuo ZX, Xia HM, et al. Investigation into the impact of diagnostic ultrasound with microbubbles on the capillary permeability of rat hepatomas. *Ultrasound Med Biol*. 2013; 39: 628-37.
44. Kopeček JA, Carson AR, McTieman CF, et al. Ultrasound Targeted Microbubble Destruction-Mediated Delivery of a Transcription Factor Decoy Inhibits STAT3 Signaling and Tumor Growth. *Theranostics*. 2015; 5: 1378-87.
45. Carson AR, McTieman CF, Lavery L, et al. Ultrasound-targeted microbubble destruction to deliver siRNA cancer therapy. *Cancer Res*. 2012; 72: 6191-9.
46. Xu J, Zeng X, Liu Y, et al. A novel dual-targeted ultrasound contrast agent provides improvement of gene delivery efficiency in vitro. *Tumour Biol*. 2016; 37: 8609-19.
47. Timmins NE, Nielsen LK. Generation of multicellular tumor spheroids by the hanging-drop method. *Methods Mol Med*. 2007; 140: 141-51.
48. Xie X, Liu W, Liu H, et al. Ultrasound-responsive nanobubbles contained with peptide-camptothecin conjugates for targeted drug delivery. *Drug Deliv*. 2016; 23: 2756-64.
49. Hu Q, Gao X, Gu G, et al. Glioma therapy using tumor homing and penetrating peptide-functionalized PEG-PLA nanoparticles loaded with paclitaxel. *Biomaterials*. 2013; 34: 5640-50.
50. Rapoport NY, Efron AL, Christensen DA, et al. Microbubble Generation in Phase-Shift Nanoemulsions used as Anticancer Drug Carriers. *Bubble Sci Eng Technol*. 2009; 1: 31-9.
51. Kripfgans OD, Fowlkes JB, Miller DL, et al. Acoustic droplet vaporization for therapeutic and diagnostic applications. *Ultrasound Med Biol*. 2000; 26: 1177-89.
52. Hirschhaeuser F, Menne H, Dittfeld C, et al. Multicellular tumor spheroids: an underestimated tool is catching up again. *J Biotechnol*. 2010; 148: 3-15.
53. Markovitz-Bishitz Y, Tauber Y, Afrimzon E, et al. A polymer microstructure array for the formation, culturing, and high throughput drug screening of breast cancer spheroids. *Biomaterials*. 2010; 31: 8436-44.
54. Chen H, Hwang JH. Ultrasound-targeted microbubble destruction for chemotherapeutic drug delivery to solid tumors. *J Ther Ultrasound*. 2013; 1: 10.
55. Zhang K, Li P, Chen HR, et al. Continuous Cavitation Designed for Enhancing Radiofrequency Ablation via a Special Radiofrequency Solidoid Vaporization Process. *ACS Nano*. 2016; 10: 2549-58.
56. Zhang K, Chen HR, Li FQ, et al. A continuous tri-phase transition effect for HIFU-mediated intravenous drug delivery. *Biomaterials*. 2014; 35: 5875-85.
57. Zhang K, Xu HX, Chen HR, et al. CO2 bubbling-based 'Nanobomb' System for Targetedly Suppressing Panc-1 Pancreatic Tumor via Low Intensity Ultrasound-activated Inertial Cavitation. *Theranostics*. 2015; 5: 1291-302.